

4.2 Mechanical Measurements

One of the most significant events during the 3rd quarter time period was a change in the ventilation in the Thermal Test Alcove which caused a cooldown in the Heated Drift. According to the Test Coordination Office, on Thursday 7/30/1998 at approximately 1130 hours, the new Alcove #5 high power ventilation system was started. As per A/E Design Drawing BABFAA000-01717-2100-44110-00, the new system delivers approximately 20,000 cubic feet per minute (CFM) to a location about 10 feet from the Thermal Bulkhead. If conditions near the bulkhead exceed 98°F (37°C), a second duct delivers another 20,000 CFM until the temperature drops below this threshold. Sometime after the system was started on 7/30/1998, the insulation that plugs the hole in the bulkhead allowing the camera rail to pass through the bulkhead became dislodged. This provided an open conduit for a large quantity of ambient air to be forced into the Heated Drift. The Heated Drift experienced a cooldown as shown by the various temperature sensors in the drift. This hole was discovered the evening of Wednesday 8/5/1998 and re-sealed. Until the hole was sealed, the air temperature in the drift had dropped from around 272°F (133°C) on Thursday to around 259°F (126°C) on Wednesday.

Temperature changes resulting from the increased ventilation through the bulkhead were observed all the way to the deep end of the drift, where decreases of 2-5°C were observed on the surface thermocouples on the concrete liner.

Another problem with temperatures was found with the TCs along MPBX-1 (Borehole 81, the long borehole parallel to the drift axis on the north side of the drift). On June 19, all the temperatures in this borehole undergo a precipitous drop, with the TCs in the deep end of the borehole dropping as much as 10 °C. For about a month afterward, the temperatures apparently rise at a higher rate. Then on July 28, the temperatures drop again, to curves which seem to be what they would have been if they had risen according to the original rates.

The second drop in temperature near July 28th is most probably related to the high power ventilation system being turned on. The first drop around June 19th is more difficult to explain. The dates do not correspond to Plate Loading Test activities, so that may be eliminated as a cause. The TCO reports that no hardware or scan changes were made to the DST DCS during this month interval. The only potentially related event uncovered thus far is that the main ESF ventilation system was shut down at about 15:00 UTC (08:00 PDT) on June 20th for 48 hours for LBNL to conduct seismic testing/monitoring in the ESF. The Alcove 5 old ventilation system continued to operate as normal.

Mechanical Data

The behavior exhibited thus far by the MPBXs continues to be similar to the elastic model predictions, with the exception of MPBX-14, which demonstrates separation between the invert and liner. The deepest anchor (Anchor #4) for the MPBXs is progressing toward having the largest displacement from the collar. Most of the MPBX sensors are working well; however, MPBX-5, -7, and -11 have gone totally bad, and MPBX-3, -6, and -14 have gotten progressively noisier during the 3rd quarter.

Due to a problem with the revision of the scan software done on August 4th, the CDEX-1 and CDEX-2 data were not read properly by the DCS for the interval from 8/4/1998 until 9/25/1998. The raw data and Q Engineering readings do not exist for these sensors during this interval. After 9/25/1998 the readings are done the normal manner.

The strain gages placed on the concrete liner and on unconstrained concrete samples in the Heated Drift continue to show the combined effects of thermal expansion, dehydration-induced shrinkage, and mechanical stress imposed by the interaction of the concrete with the heated rock surrounding the drift. The results from the strain gages on the unconstrained samples exhibit behavior indicative of drying shrinkage due to dehydration, a phenomenon seen elsewhere in engineering literature. The circumferential

strain gages on the liner consistently show that the crown of the liner is in compression while the rest of the liner experiences smaller magnitudes of compression and tension.

The strain gage and liner surface temperature gage data experienced precipitous drops starting on July 30 and lasting 3-4 days due to the new high power ventilation system in Alcove 5. The temperatures dropped 2-5°C, and the strains dropped by 20-100 microstrains, as high as 15% of their values before the drop. These values recovered after the bulkhead was re-sealed on August 5.

4.2.1 Rock Thermal Expansion

The coefficient of thermal expansion (CTE) of repository horizon rocks, especially the middle non-lithophysal sub-unit (Tptpmn) of TSw2, have been measured extensively in the laboratory using small hand samples which can be taken to be intact rock. In earlier years, these tests were done on samples obtained by surface-based drilling. Recently, laboratory testing for thermal expansion has been carried out on samples from the SHT and DST test blocks as well as the thermal test alcove in general. Measurements have been made on both pre-heating and post-heating samples for the SHT and only pre-heating samples for the DST. The results of lab measurements of CTE associated with the SHT and DST are shown in Figure 4.2-1. In this figure, CTE in $10^{-6}/^{\circ}\text{C}$ is plotted against temperature. As the plots show, below 200°C lab measured CTE of Tptpmn is approximately 10×10^{-6} . Above 200°C however, CTE dramatically increases, by as much as a factor of 5 or 6 at 300°C. This sharp increase in lab measured CTE above 200°C is thought to be due to volume changes associated with phase changes of silica polymorphs above approximately 230°C.

It is recognized that in a fractured rock formation, the CTE of the rock mass would be less than that of the intact rock as measured in the laboratory. The extent of the decrease is thought to depend on the scale at which measurements are made as well as the temperature level. Measurements of the displacements in the rock during the heating in the SHT and the DST provide an opportunity to derive values for rock mass CTE at various gage lengths (scales) and levels of temperatures. Values of the CTE of Tptpmn thus derived are presented in Table 4.2-1 along with relevant lab measured value. The data in Table 4.2-1 show that rock mass thermal expansion as measured by the SHT and DST are substantially lower than the lab measured CTE of intact rock.

Rock mass CTE values from Table 4.2-1 are plotted in Figure 4.2-2 to show the relationship between CTE and temperature in Figure 4.2-2a and that between CTE and gage length in Figure 4.2-2b. Figure 4.2-2 clearly shows that CTE increases, as expected, with the increase in temperature. The database for gage length is not adequate. Nonetheless, the expected trend of decreasing CTE with increasing gage length is there.

Table 4.2-1. Comparison of Rock Mass Matrix Thermal Expansion

Test Name	Gage Length (m)	Average Temp./Temp. Range (°C)	Coefficient of Thermal Expansion ($10^{-6}/^{\circ}\text{C}$)
Single Heater Test	2.84	160	5.88
Single Heater Test	4.14	70	4.14
Single Heater Test	2.36	116	3.4
Drift Scale Test	7	25-50	1.65
Drift Scale Test	7	50-75	2.51
Drift Scale Test	7	75-100	3.25
Laboratory	0.1	25-200	-10

Figure 4.2-1. Increase in Thermal Expansion Above 200°C. Due to silica Phase Change

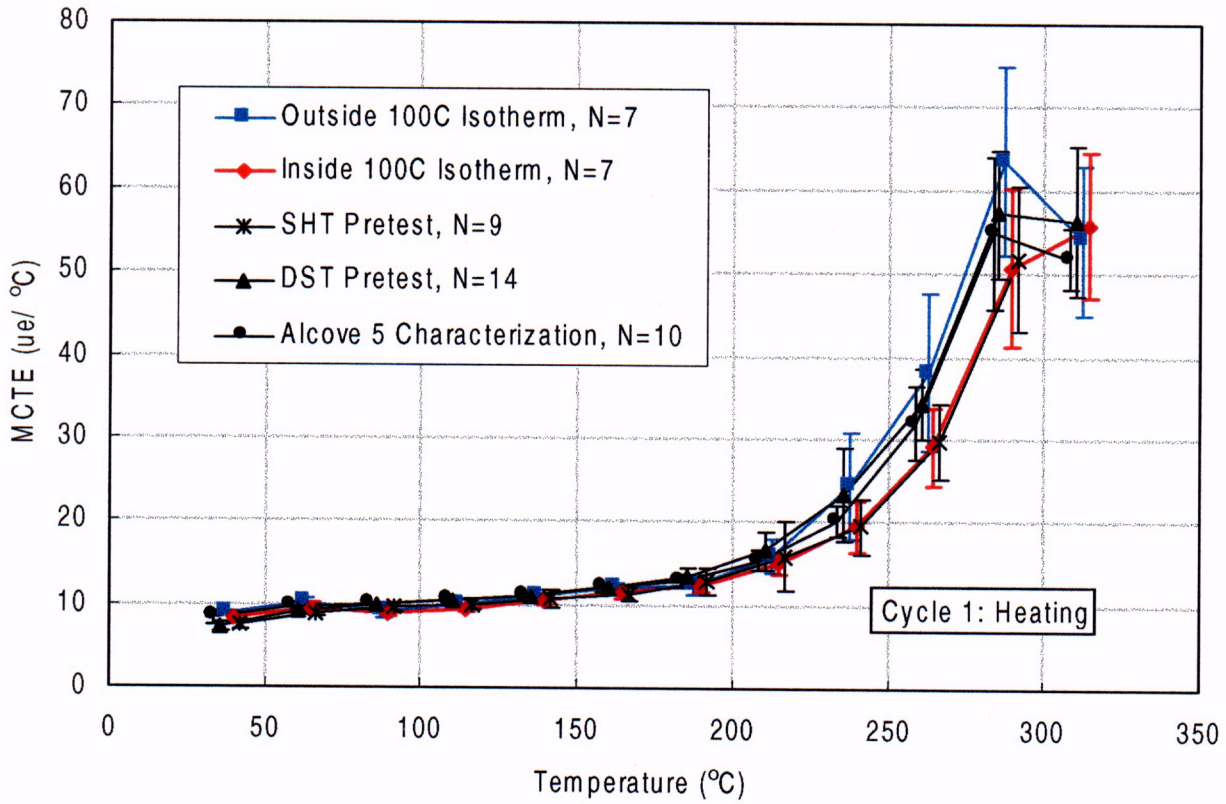
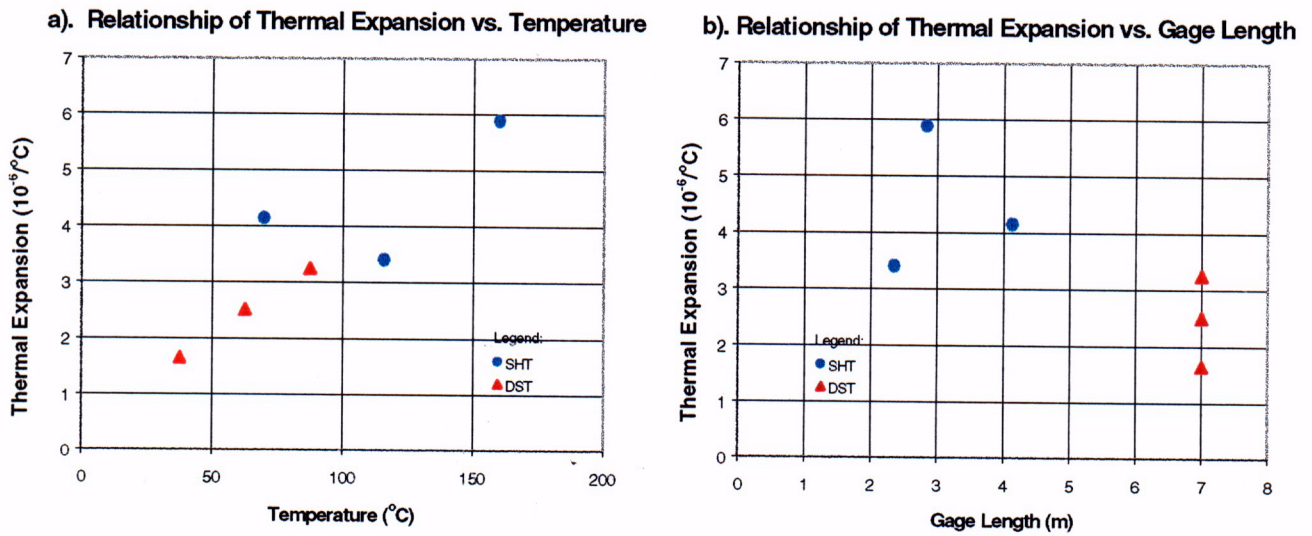


Figure 4.2-2. Relationship of Thermal Expansion vs. Temperature (a) and Gage Length (b)



C-15

4.3 Air-K and Gas Tracer Tests

Input to progress report on ESF thermal test, November, 1998 from Yvonne Tsang on Hydrological measurements in the Drift Scale Test

The most prominent thermal-hydrological processes anticipated in the Drift Scale Test (DST) is the redistribution of moisture by vapor transport and subsequent condensation. Air injection tests in 4 consecutive zones in each of the twelve hydrology holes, carried out at approximately three month intervals, are intended to monitor the changes in liquid saturation in the fractures due to vaporization and condensation. In particular, results of the air injection tests are used to locate those zones where liquid saturation in the fracture has increased, thus giving rise to a reduction in the local permeability value. In Figures 4.3-1 and 4.3-2 are shown the air permeability of respective zones in the hydrology boreholes, measured at different stages of the test up to 9 months of heating. The permeability is plotted as a ratio with respect to their respective pre-heat November 1997 values. Only those measurements which indicate more than a reduction of 10% (precision of air injection measurements) are shown in Figures 4.3-1 for zones in boreholes 57 through 61, and in Figure 4.3-2 for zones in boreholes 74 through 78. Borehole sections where decrease in permeability were measured at different stages of heating as displayed in Figures 4.3-1 and 4.3-2 are consistent with those condensation zones predicted from the numerical model (Birkholzer and Tsang, 1998). The simulated fracture liquid saturation at 3, 6, and 9 months of heating are shown in Figures 4.3-3 and 4.3-4, in the xz cross sections containing the fan of boreholes 57 through 61, and the fan of boreholes 74 through 78 respectively. Denotation for borehole sections by borehole number follow by the zone number in Figures 4.3-1 and 4.3-2 are such that zone 1 refers to the borehole section closest to the borehole collar, and zone 4 refers to the borehole section between the fourth packer and the bottom of the borehole. In Figures 4.3-3 and 4.3-4 the locations of the packers in the boreholes are denoted by the white circles. In most boreholes the first packer closest to the collar is off-scale, the exception is borehole 58, where only 3 packers were installed and therefore 58-3 refers to the borehole section between the third packer and the bottom of the borehole. Furthermore, in borehole 77, of the three packers installed, the third packer has been damaged and deflated since March 1998, leaving essentially only one zone, 77-1 for which air permeability measurements are meaningful. Simulated results in Figure 4.3-4 show that saturation build-up in the fractures occur in zones 60-2 and 61-2 as early as 3 months after initiation of heating. As heating progress to 6 and 9 months, condensation also extends to 60-3, 60-4, 61-3, and eventually to those boreholes above the heated drift, 59-2, 59-3, 59-4, as well as in 58-1 and 58-2. Air permeability data in Figure 4.3-1 indicate that the only borehole sections which show decrease in permeability are 60-2, 3, 4; 61-2, 59-2, 3 and 58-2. The measured permeability in 58-2 and 60-4 show an initial large decrease, then subsequent rise (though not reaching their pre-heat values) as the heater test progresses. This behavior is not anticipated in the simulated results based on a homogeneous description of the fracture continuum. It can be caused by gravity drainage through fractures after an initial build up of condensation; drainage can be expected to be spatially heterogeneous, since fracture can have different orientations, and are of different length scales. Data in Figure 4.3-2 show that zones of decreased air permeability occurred in boreholes 78 and 76 for the first 9 months of heating, which is again consistent with the predicted fracture liquid saturation at 3, 6, and 9 months of heating shown in Figure 4.3-4.

Though air-injection tests in the hydrology holes were intended mainly to locate zones of increased fracture liquid saturation from condensation, post-test characterization of the Single Heater Test have indicated an overall increase in air permeability in the test block which may be attributed to microfracturing. For this reason, the air permeability data in the Drift Scale Test were also studied to unveil any thermal-mechanical coupled effects. We screened our data to investigate only those upward inclining boreholes that are farthest from the heaters, i.e. boreholes 57 and 74, where condensation was not yet anticipated at 9 months of heating. The measurements do show an increase in permeability during tests for zones 57-3, 57-4 and 74-4. These and air-injection data yet to be collected as the heating phase progress will be studied closely in order to sort out the thermal-hydrological and thermal-mechanical coupled processes.

Gas tracer tests in boreholes 74, 75 and 76 have indicated an effective fracture porosity on the order of 0.01. This values is orders of magnitude higher than what is deduced from a parallel plate conceptualization of fractures together with the ESF fracture mapping data. It was suggested that the large value of fracture

porosity perhaps arises from the connected pore space of the lithophysal cavities that seem pervasive in the DST according to the borehole videos. During this quarter gas tracer tests have been carried out in Niche 3107 in the ESF. Niche 3107, though in the same middle non-lithophysal welded tuff unit as the DST, is rather intact. While in the DST area the tracer tests were carried out in borehole sections of 8 to 9 meters, in Niche 3 the corresponding length of the borehole section was less than 1 m. The estimated fracture porosity from gas tracer tests in Niche 3 is 0.012-0.02, again on the order of 0.01 as was measured for the DST. The rather consistent fracture porosity of 0.01 at different locations, on different length scales, and for welded tuff of apparently different fracture characteristics, indicate that fractures in the Topopah Spring welded tuff in fact occupy a pore space on the order of 1%, which is considerably larger than previously estimated from fracture mapping data, thus implying that transport in the fractures of the proposed repository middle nonlithophysal unit would be one or two orders of magnitude slower than transport estimated using previously calculated fracture porosity.

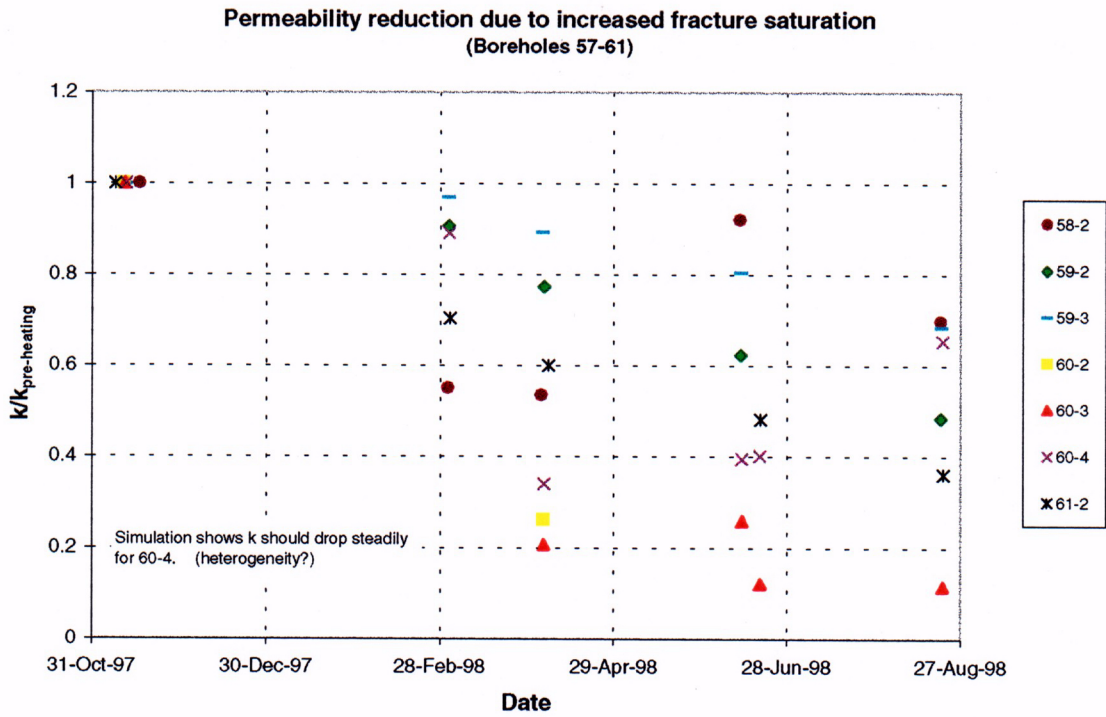


Figure 4.3-1 Decrease in measured air permeability (normalized to respective pre-heat values) due to increase liquid saturation for zones in boreholes 57 through 61.

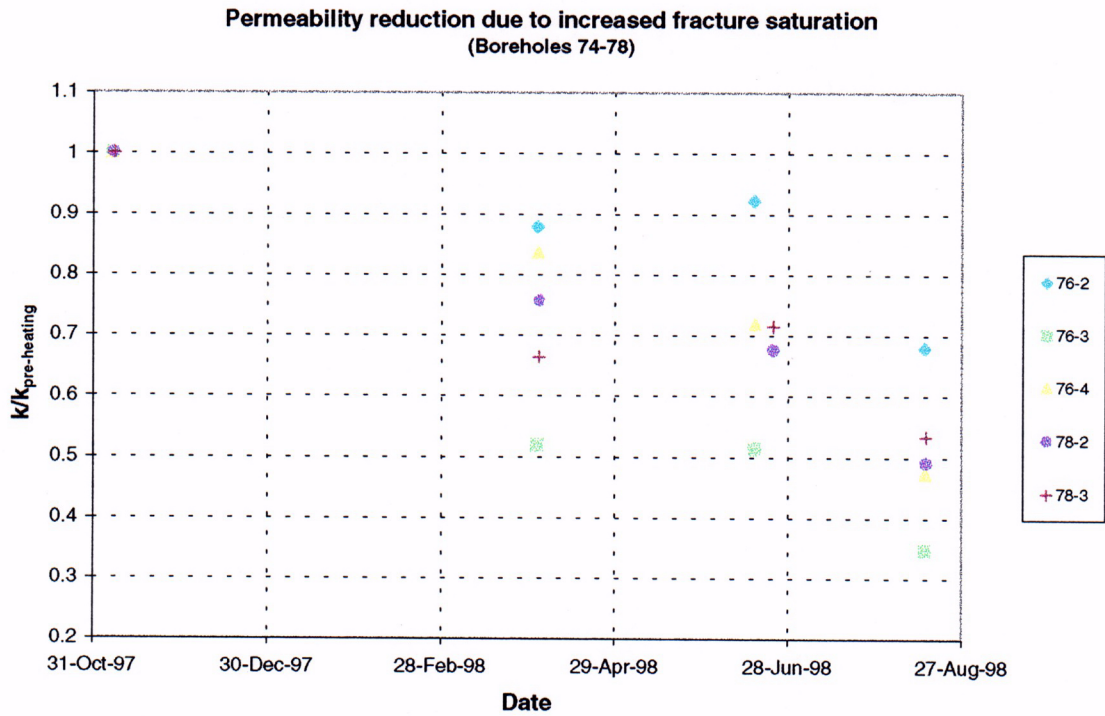


Figure 4.3-2 Decrease in measured air permeability (normalized to respective pre-heat values) due to increase liquid saturation for zones in boreholes 74 through 78. (DTN:LB981016123142.002)

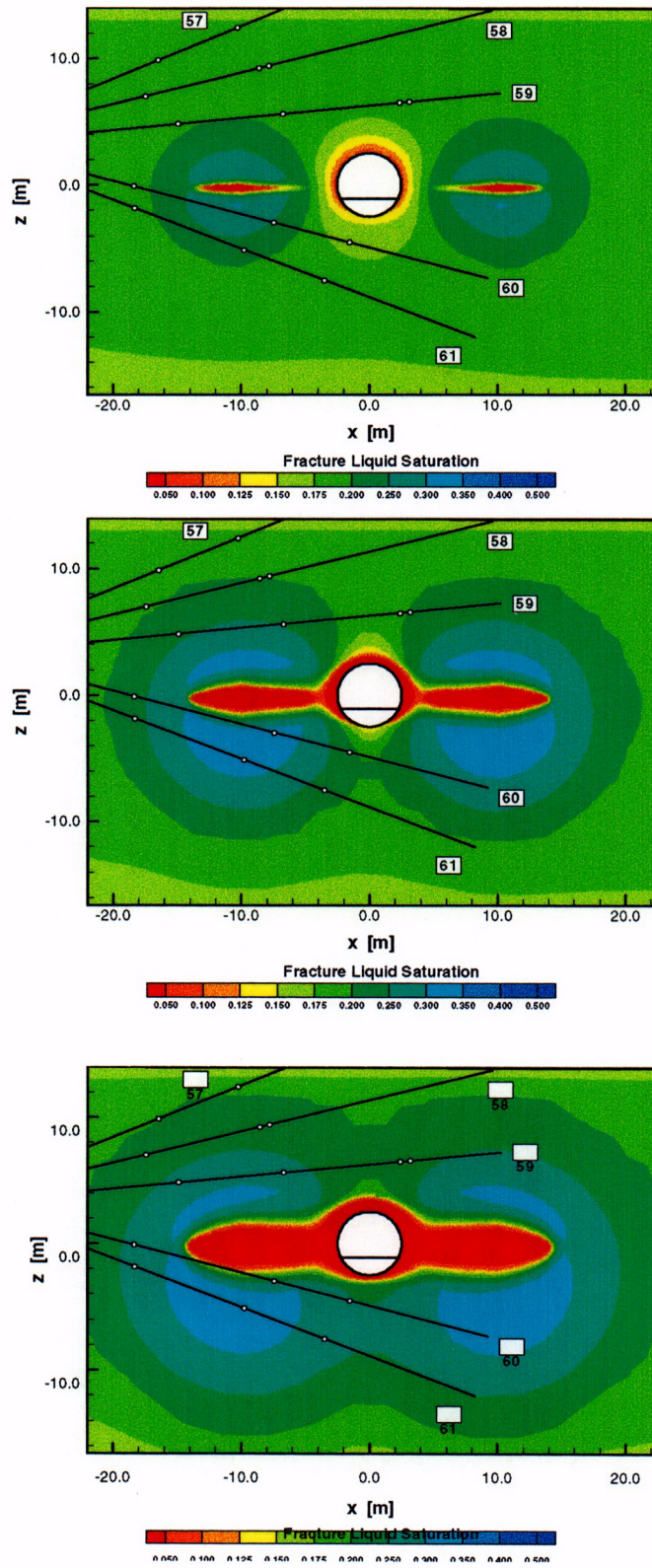


Figure 4.3-3 . Simulated fracture liquid saturation at 3 (top), 6, and 9 (bottom) months after heating in boreholes 57 through 61.

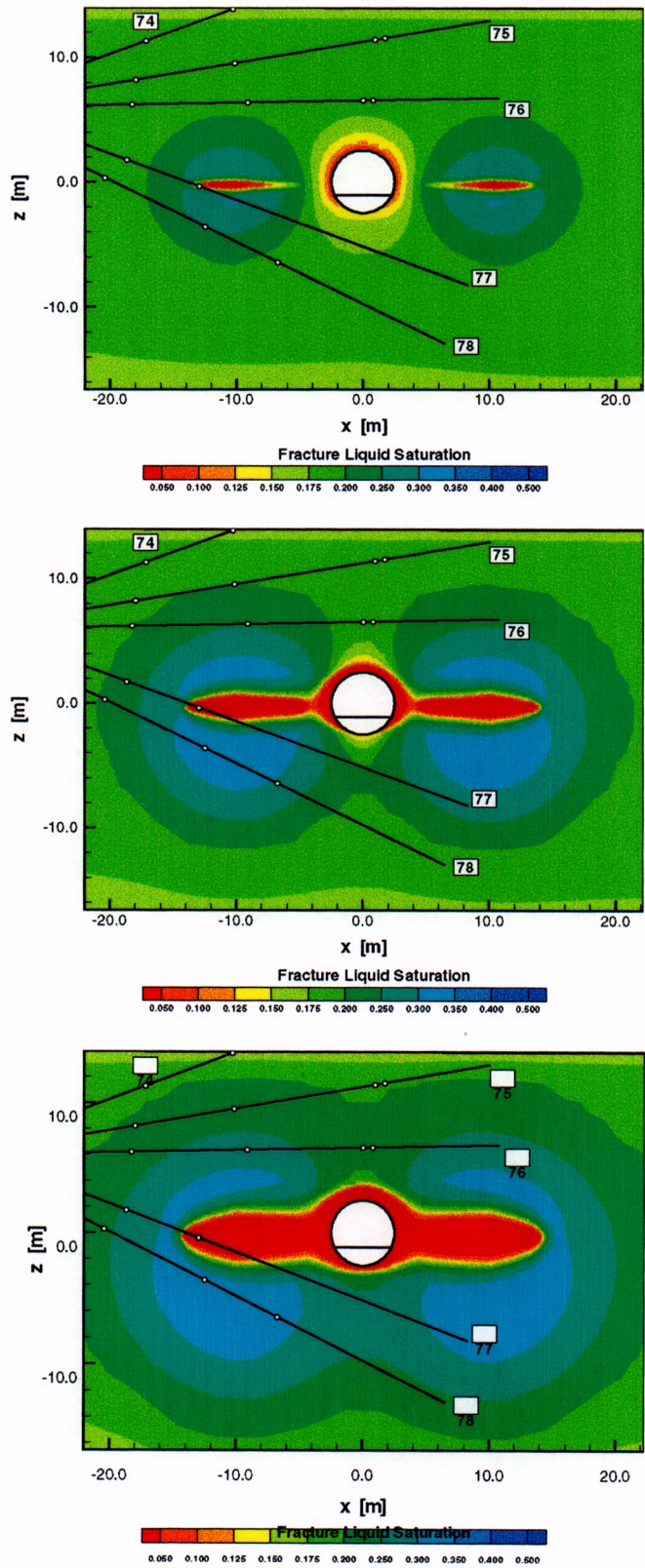


Figure 4.3-4 Simulated fracture liquid saturation at 3 (top), 6, and 9 (bottom) months of heating for boreholes 74 through 78

C-18

4.4 ERT MEASUREMENTS

Electrical Resistivity Monitoring of the Drift Scale Test: June-August, 1998

A. Ramirez, W. Daily

Introduction:

This letter report describes electrical resistance tomography (ERT) surveys made at the Drift Scale Test (DST), during the June to August, 1998 time period. ERT is one of the several thermal, mechanical, and hydrologic measurements being used to monitor the rock-mass response during the DST. The purpose of this work is to map the changes in moisture content caused by the heating of the rock mass water, with a special interest in the movement of condensate out of the system..

The purpose of this letter report is to provide a brief synopsis of the progress made during the time period of interest. A comprehensive discussion of the process followed to produce the results shown here, equipment used, and assumptions made can be found in Wagner, 1998, pages 7-13 to 7-21.

Changes in Electrical Resistivity:

Tomographs of resistivity change corresponding to the time period between June 3, 1998, and August 18, 1998, are shown in Figures 4.4-1, 4.4-2, and 4.4-3. The top part of each of these figures shows the tomographs collected along a cross-section parallel to the Heated Drift (HD). The lower left portion of the figures shows tomographs corresponding to a vertical plane intersecting the HD at right angles, and about 5 meters in from the bulkhead; we will refer to this plane as AOD 1. The lower right portion of the figures corresponds to a second vertical plane intersecting the HD at right angles, about 24 meters in from the bulkhead; we will refer to this plane as AOD 5.

The upper part of Figure 4.4-1 shows the changes in resistivity along the HD, calculated after 182 days of heating. Note that most of the tomographs are yellow-green in color, thereby indicating resistivity ratios near 1.0 (no change relative to the pre-heat case). Near the walls of the HD, the tomographs show resistivity ratios less than 1.0, thereby indicating that the resistivity has decreased relative to the pre-heating condition. After 224 days of heating (upper portion of Figure 4.4-2), most of the rock still shows a ratio of 1.0, but the rock near the crown and invert of the HD shows stronger resistivity decreases (ratios farther removed from 1.0). These decreases become stronger as heating time increases (upper portion of Figure 4.4-3). The tomographs also indicate that the resistivity changes above the HD are stronger than those below the HD. We believe that these resistivity changes are due primarily to increases in temperature that have developed close to the walls of the HD.

The lower left portions of Figures 4.4-1, 4.4-2 and 4.4-3, shows the tomographs corresponding to AOD 1. Although the mesh consists of a large region around the electrode arrays, only the region inside the ERT electrode array is shown in the figure because the region outside the array is poorly constrained by the data. The region inside the HD is also masked because the technique does not measure rock properties in the excavated region. The tomograph sequence shows a region of resistivity decrease near the walls of the HD. The resistivity decreases become stronger with time and they extend farther into the rock above the HD. Surprisingly, the region corresponding to the wing heaters location (nine o'clock position relative to the HD) shows relatively weak resistivity decreases.

The lower right portions of Figures 4.4-1, 4.4-2 and 4.4-3, depicts resistivity-change tomographs sampling the rock mass along AOD 5, which is a second vertical plane that intersects the HD at right angles near its middle. The images show both increases (ratios greater than 1.0) and decreases near the location of the wing heaters. Resistivity decreases are also observed near the walls of the HD. We suggest that the resistivity changes observed through August, 1998, are caused by temperature increases as well as saturation decreases. The AOD 5 results in Figures 4.4-1, 4.4-2 and 4.4-3 make it clear that resistivity increases are observed in the rock closest to the wing heaters while resistivity decreases are observed

farther away. This behavior is caused by the competing effects that saturation decreases and temperature increases have on electrical resistivity. In rock where rock temperature has increased but relatively little drying has occurred, the resistivity will decrease because the temperature increase has enhanced the mobility of the ions in the pore water. As significant drying occurs and the saturation is higher than about 30%, the pore water paths through which electrical charge moves become smaller, thereby tending to increase the water resistivity. However, the net change in bulk resistivity is a decrease relative to baseline because the increases in ion mobility more than compensate for the volumetric reduction of the pore water pathways. As the temperature continues to increase and the saturation drops below 30%, the pore water paths through which electrical charge moves starts to become discontinuous. This makes the bulk resistivity increase exponentially even though the increases in ion mobility caused by temperature are still present. Thus, the net effect on the bulk resistivity is an increase above baseline (i.e., the ratio becomes greater than 1.0) in hot dry rock with saturations less than 30%.

There are both similarities and differences between the AOD 1 and AOD 5 planes. Both show resistivity decreases, near the walls of the HD, that extend deeper into the rock above the crown of the HD than below its invert. A significant difference between the AOD 1 and AOD 5 results is observed in the vicinity of the wing heaters where the AOD 1 tomographs show weaker decreases in resistivity near the bulkhead. Possible reasons for this difference can be found in Wagner, 1998.

Estimates of Saturation Change:

The resistivity changes shown in Figures 4.4-1, 4.4-2 and 4.4-3 are influenced by changes in moisture content, temperature, and ionic strength of the water. To estimate saturation, it is assumed that the dominant factors affecting resistivity changes are temperature and saturation. That is, an increase in temperature or water saturation causes a resistivity decrease. Near the heaters, there may be regions where the increasing temperature reduces the resistivity, while rock drying changes the resistivity in the opposite sense (increases the resistivity). Our goal in this section is to use the images of resistivity change near the HD, along with the measured temperature field and what is known of initial conditions in the rock mass, to estimate moisture change during heating. A detailed description of this approach can be found on a previous milestone report pertaining to the Single Heater Test (Ramirez and Daily, 1997).

To estimate moisture content changes, the effects of both rock temperatures and resistivity changes measured by ERT must be taken into account. Interpolation of temperature measurements made at discrete points was necessary to develop the temperature fields showing temperature values at each tomograph pixel. The interpolations can sometimes be in error when the interpolation algorithm is not sufficiently constrained by the measured values and because the interpolation does not necessarily satisfy physical laws.

Note that the temperature estimates were generated following a *nonqualified* process; therefore, the saturation estimates are *nonqualified*. Also, the saturations estimates are considered approximate, as indicated later in this report.

Figures 4.4-4, 4.4-5, and 4.4-6 show the saturation change estimates corresponding to heating days 182, 224, and 258 respectively. The results shown were calculated using Model 2 as described in Ramirez and Daily (1997). Model 1 results are not shown in order to be concise. Note that the Model 2 estimates on Figure 4.4-4 indicate that most of the rock immediately adjacent to the HD and to the wing heaters show saturation ratios below 1.0. These estimates suggest that some drying is occurring close to the HD. A lot more drying is occurring close to the wing heaters. Also note that the drying zone is growing very slowly with time. The tomographs suggest that the drying zone extends farther into the rock above the HD and than below it. The saturation ratio estimates shown in Figure 4.4-6 suggest that the rock showing the maximum amount of drying is located in plane AOD 5, forming a horizontal zone centered on the wing heaters. The tomographs show that this zone has lost about four-fifths of its water (saturation ratio of about 0.20) by mid-August, 1998. When compared to AOD 1, AOD 5 shows a stronger zone of drying that extends beyond the zone where the wing heaters are located.

Saturations ratios greater than 1.0 indicate regions in the rock where water saturation is increasing relative to the pre-heating conditions; we will refer to these zones as wetting zones. Wetting zones are observed in

Figures 4.4-4, 4.4-5, and 4.4-6. Most of these occur below the HD, near the bulkhead as well as in discrete zones closer to the middle of the HD. Another wetting zone appears above and near the edge of the wing heater location, within plane AOD 5.

All of the saturation estimates presented are considered to be approximations. The accuracy of the saturation estimates in may be limited by one or more of the factors listed in Wagner, 1998.

References:

Ramirez, A., and W. Daily (1997). *Electrical Resistivity Monitoring of the Thermomechanical Heater Test in Yucca Mountain*. Milestone report for the CRWMS Management and Operating Contractor, U.S. Department of Energy. (SP9215M4) Livermore, CA: Lawrence Livermore National Laboratory.

Wagner, R., 1998, Drift Scale Test Progress Report No. 1 (BAB000000-01717-5700-00004, Draft A), August 1998, TRW Environmental Safety Systems Inc., Las Vegas Nevada.

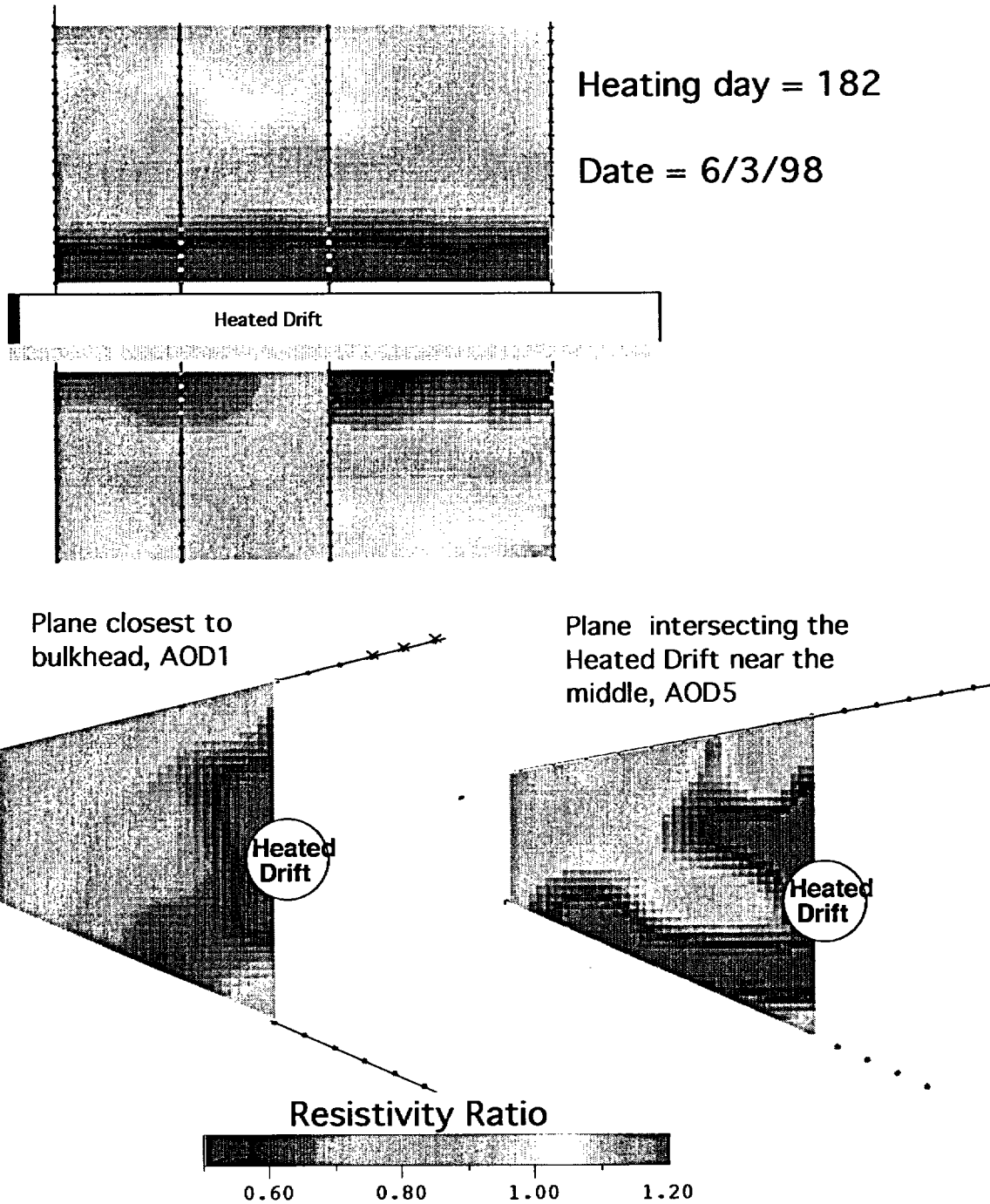


Figure 4.4-1. Tomographs of electrical resistivity ratio for heating day 182. The tomographs show changes relative to the preheating (November 18, 1997) electrical resistivity distribution. A resistivity ratio equal to 1.0 indicates no change; values less than 1.0 indicate that the resistivity is decreasing relative to the baseline.

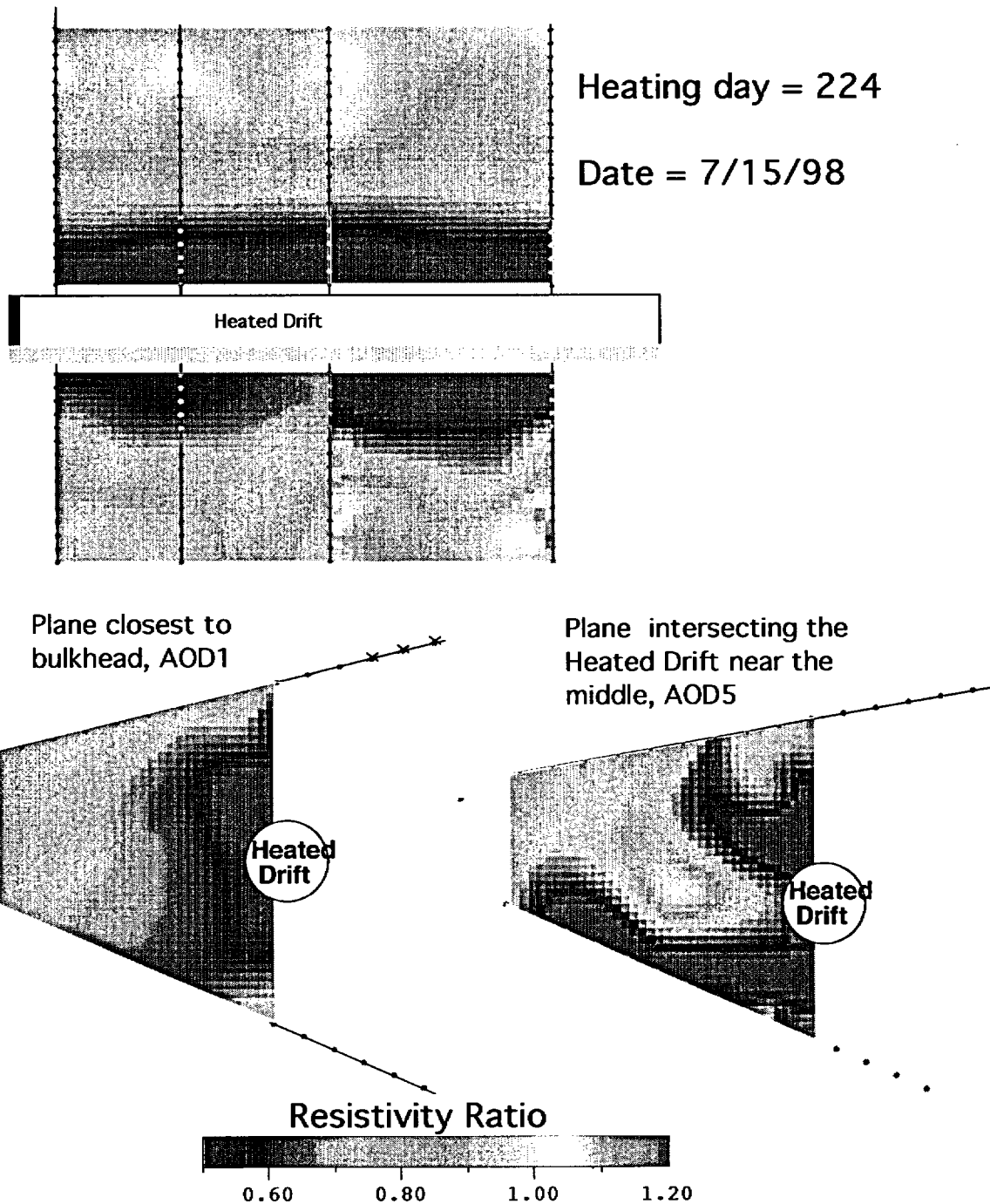


Figure 4.4-2. Tomographs of electrical resistivity ratio for heating day 224. The tomographs show changes relative to the preheating (November 18, 1997) electrical resistivity distribution. A resistivity ratio equal to 1.0 indicates no change; values less than 1.0 indicate that the resistivity is decreasing relative to the baseline.

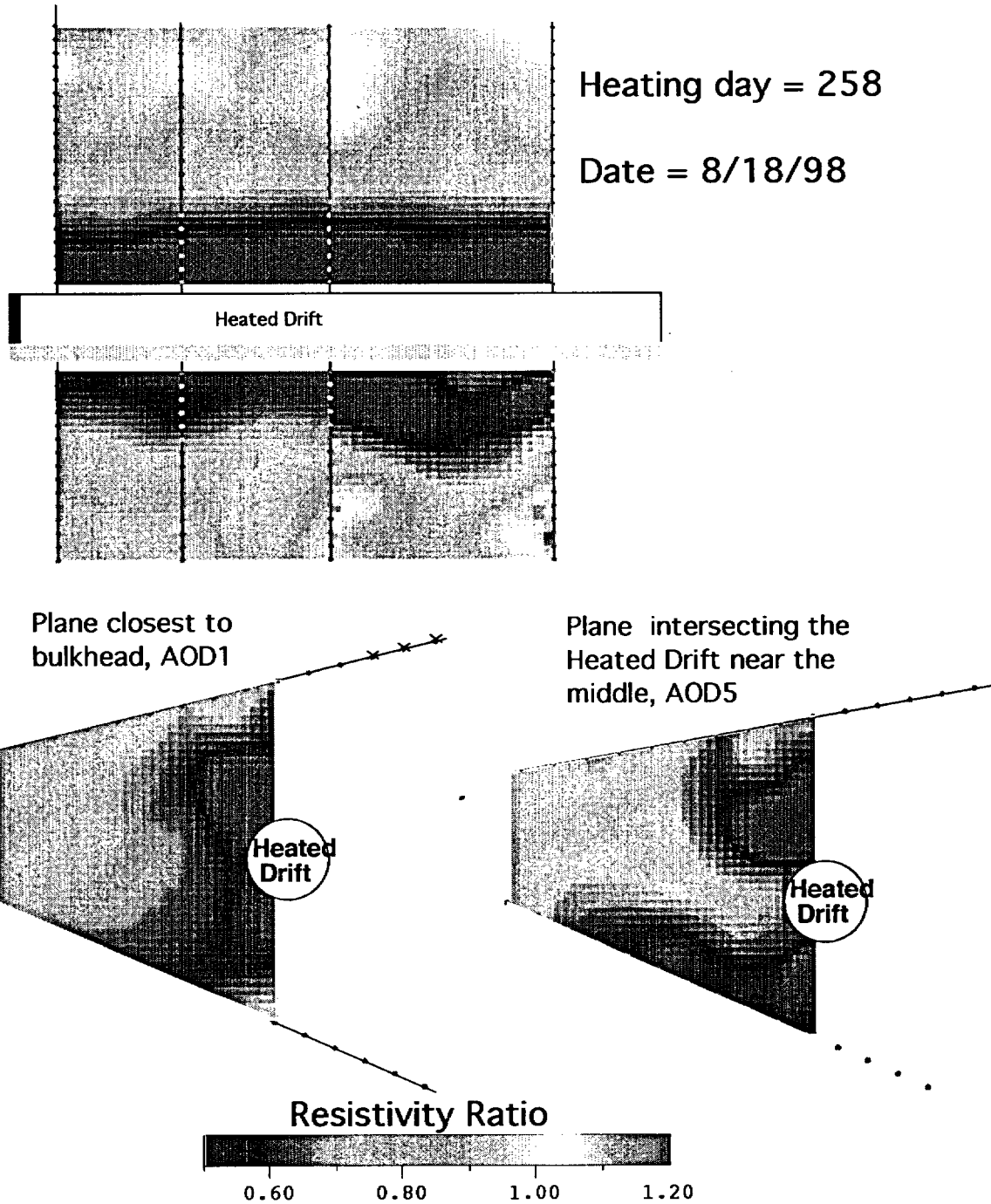


Figure 4.4-3. Tomographs of electrical resistivity ratio for heating day 258. The tomographs show changes relative to the preheating (November 18, 1997) electrical resistivity distribution. A resistivity ratio equal to 1.0 indicates no change; values less than 1.0 indicate that the resistivity is decreasing relative to the baseline.

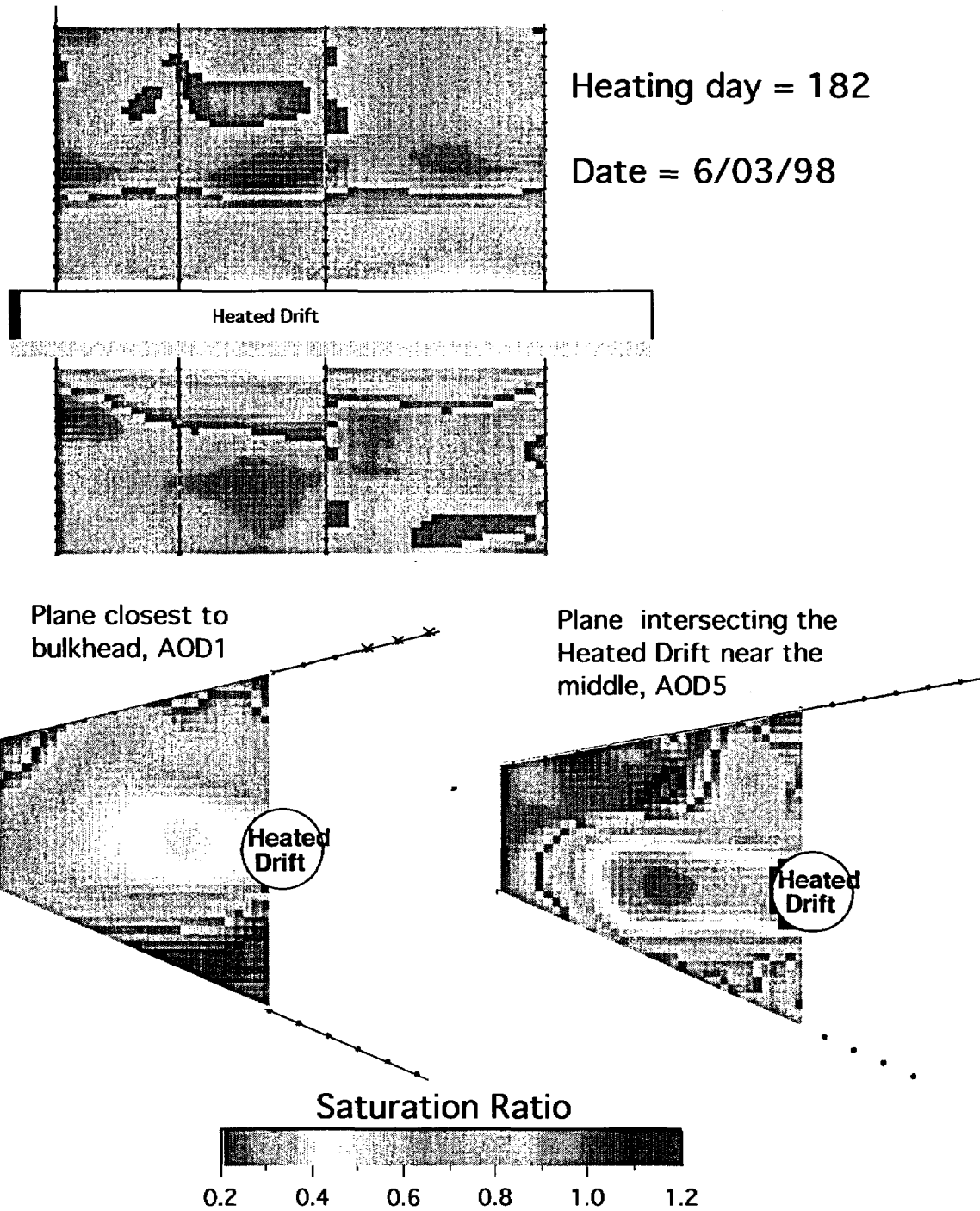


Figure 4.4-4. Tomographs of saturation ratio for heating day 182. The tomographs show changes relative to the preheating (November 18, 1997) saturation distribution. A saturation ratio equal to 1.0 indicates no change; values less than 1.0 indicate that the saturation is decreasing relative to the baseline.

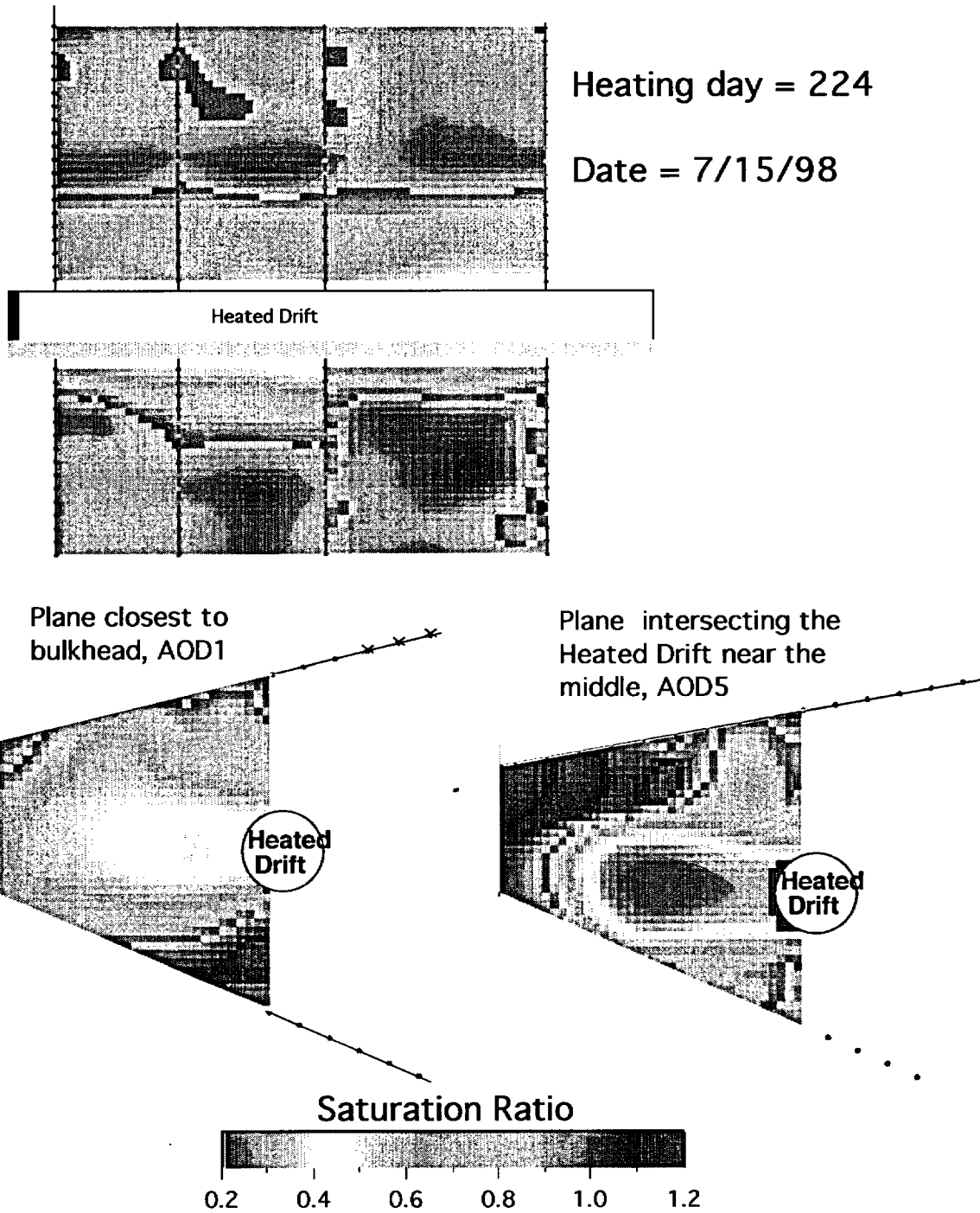


Figure 4.4-5. Tomographs of saturation ratio for heating day 224. The tomographs show changes relative the preheating (November 18, 1997) saturation distribution. A saturation ratio equal to 1.0 indicates no change; values less than 1.0 indicate that the saturation is decreasing relative to the baseline.

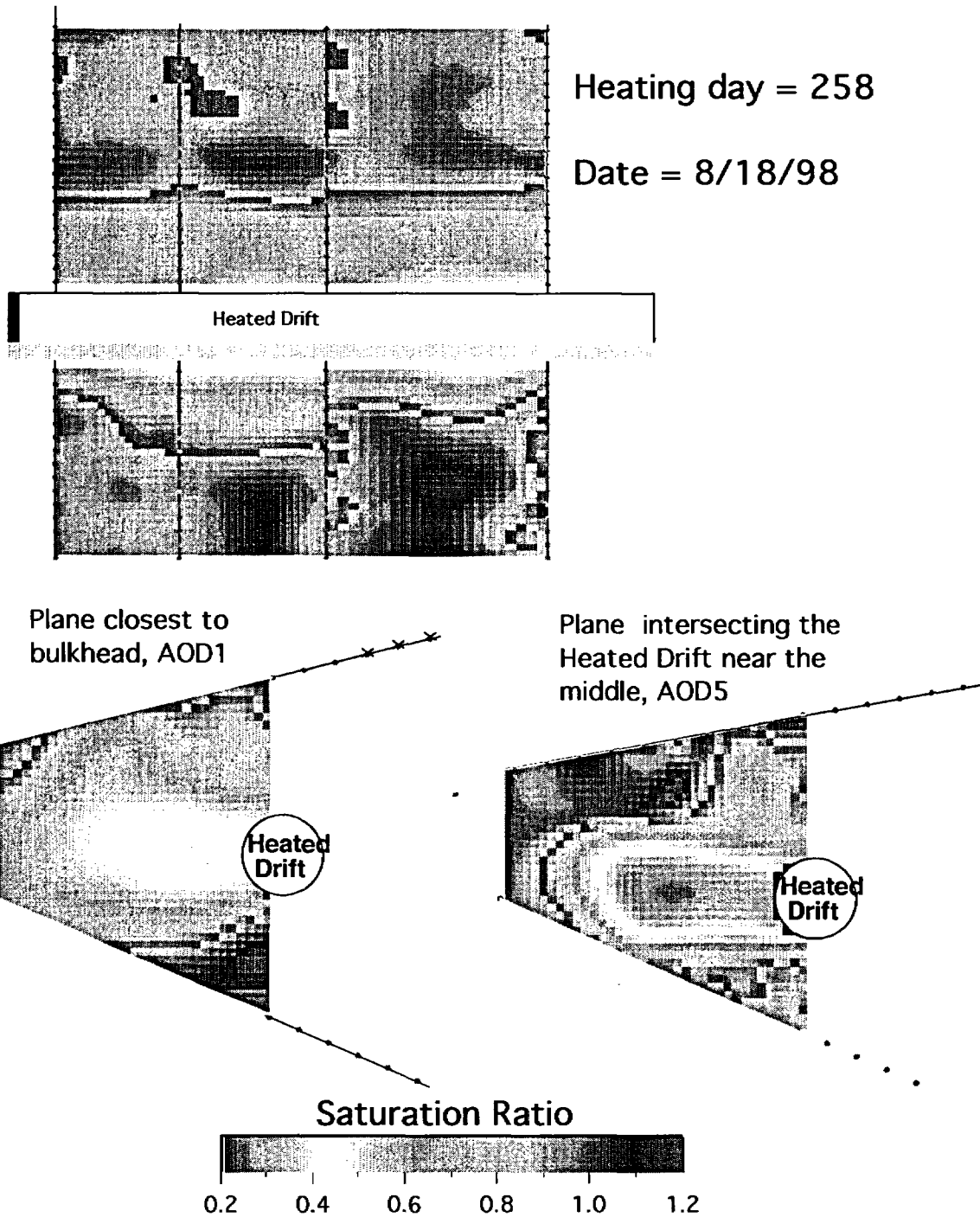


Figure 4.4-6. Tomographs of saturation ratio for heating day 258. The tomographs show changes relative to the preheating (November 18, 1997) saturation distribution. A saturation ratio equal to 1.0 indicates no change; values less than 1.0 indicate that the saturation is decreasing relative to the baseline.

4.5 GROUND PENETRATING RADAR MEASUREMENTS

Over the past several months, a variety of problems have been encountered by the ground penetrating radar (GPR) data acquisition system in support of the Drift Scale Test. The high temperatures present in several of the boreholes have resulted in equipment failures prohibiting successful and timely radar data acquisition. Specifically, it appears that the high temperatures resulting from the close proximity of the boreholes to the wing heaters directly short the radar antennas along weak points and cable connections. Much effort has been expended in determining the exact location of such weak points.

Initially, the focus of our attention was the cable head connection joining the dipole antenna to the coaxial lead-in cable. It was believed that by removing this potential failure point the system would resume normal operation – even at greatly elevated temperatures. A preliminary design was built and tested with no cable head connection. The results were extremely encouraging: the antennas were operated at the highest borehole temperatures with no loss in signal strength or transmitter amplitude over periods of time longer than those expected during normal data acquisition. It should also be noted that although the coaxial cable was not rated for the expected temperature (140°C), it performed acceptably and within the standards specified by the manufacturer. Additionally, a small scale GPR survey was undertaken using the prototype system in four of the hottest boreholes (Borehole Numbers 50-51 and 67-68). Because of problems with cable availability, the cables were shorter than the length necessary for a complete survey. As such, the survey was conducted from roughly 23.0 to 18.0 meters down the boreholes. Fortunately, this region is associated with the highest borehole temperatures and the greatest degree of formation drying. Results appear encouraging from a data quality standpoint but final data analysis and interpretation is still underway.

Based on these results, a final design was settled upon and the modified antenna system was fabricated. Unfortunately, cable availability again became a problem and a decision was made to utilize existing coaxial cable for the modified design. The available cable was that coaxial cable previously used at the Drift Scale Test. It was believed that the weak points in this cable were confined to the region nearest the cable head connection. A portion (1-2 meters) of the existing coaxial cable was removed and the dipole antenna directly connected to the shortened cable resulting in a design that would perform similarly to the prototype design and be of a length suitable for the Drift Scale Test survey (35 meters). Subsequent testing proved that our assumptions were partially incorrect. The new antenna design again failed to function properly when subjected to the elevated borehole temperatures. It became clear, however, that temperature was not the only factor in causing antenna failure. Cable stress also appeared to play a role. The first two radar surveys completed at the Drift Scale Test were accomplished by using aluminum push rods to forcibly locate the radar antennas to a desired depth. Especially in the steeply inclined boreholes, the emplacement of the antennas likely caused damage to the coaxial cable at those points where the push rods were strapped to the cable. This location varied depending on the inclination of the borehole and the depth of the survey, and as a result, multiple locations have probably been affected. Thus, when these damaged cable locations were placed under stress and elevated temperatures, electrical shorting and antenna failure was the result (i.e. low or no signal strength).

The failure of the existing cable has forced the procurement and assembly of a new system. The design of the system is to be identical to the one specified above with one notable exception. The new cable will be composed of coaxial cable rated to high-temperature (200°C) covered in a rugged, abrasion-resistant coating also rated for high-temperature (200°C). Additionally, as part of an effort designed to develop a less damaging method for emplacing the radar antennas in the boreholes, a locking pulley system was conceived and built. This device now allows us to lock (and later remove) a pulley at 40 meters depth down a borehole. Using this pulley and an attached high-temperature string, we are able to gently and efficiently pull an antenna to a desired depth. This has proven to be extremely successful and will be very valuable in reducing cable damage in the future. It is now believed that by utilizing the undamaged, high-temperature coaxial cable along with the locking pulley system, the means exists to successfully resume GPR data acquisition in support of the Drift Scale Test.

4.6 Neutron Logging Measurements

There are twelve holes in the Drift Scale Test for measuring the moisture content of the rock by neutron logging. Ten of these holes in two fans transversely orthogonal to the Heated Drift are from the observation drift. The other two holes are drilled from the connecting drift, parallel to the Heated Drift (HD) at approximately 1m above its crown and approximately 9.5m from the centerline of the HD on either side of it.

A teflon tube is grouted in the neutron holes to facilitate movement of the probe. Since the grout contains moisture, the neutron logging system needs to be calibrated in simulated rock of known moisture content and hole and teflon tube of same diameter and same grout conditions. The neutron count from the logging is processed using the calibration data to yield moisture content of the rock. Although logging in the DST are being performed regularly since before the start of heating, calibration of the tool is not complete. For this reason, true moisture content of the logged intervals in the DST is not yet available. All actual test runs associated with the calibration of the DST neutron tool have been completed and the data is being processed at this time. Data on the true moisture content of the rock will be available in the near future.

Notwithstanding the above, preliminary qualitative conclusions regarding the drying of the rock can be made by analyzing the neutron count obtained by logging. Such analyses indicate that the rock surrounding some sections of neutron holes # 4 , 9 and 12 has been drying. Both neutron holes #4 and 9 are down holes and the drying sections not far from the outer segment of a nearby wing heater. Neutron hole #12 is parallel to the HD and the drying section in this hole is also due to wing heaters below it.

4.7 GAS SAMPLING AND ANALYSIS

Introduction

CO₂ concentrations in the rock around the Heater Drift have increased significantly since the initiation of heating. Numerical models of the system indicate that the source of this CO₂ is exsolution of dissolved inorganic carbon compounds (DIC) such as CO₃⁼, HCO₃⁻ and dissolved CO₂ from the pore waters in the rock during heating. With ~90% of the pore space in the rock filled with water, the capacity of the water to hold carbon in the form of DIC is much greater than the capacity of gas phase to hold CO₂ (on the order of 100 times as much, depending primarily on the pH and temperature). As the temperature rises, the partitioning of inorganic carbon between the gas and liquid phases shifts, with a higher proportion going into the gas phase. When the rock reaches the boiling point of water, the CO₂ concentrations will increase even more quickly until the rock dries out and all the inorganic carbon goes into the gas phase. The changing DIC concentrations in the pore fluids will have a significant impact on the chemistry of the pore fluids (especially on pH), which could strongly affect which mineral phases will be dissolved or precipitated.

The stable carbon isotopic ratios ($\delta^{13}\text{C}$ values) of CO₂ from around the heater drift have been measured in order to confirm the source of the increased CO₂ and to constrain parameters such as the changing pH of the pore waters and the nature of gas transport in the heated rock. This is possible because CO₂ and DIC in carbon isotopic equilibrium will have different $\delta^{13}\text{C}$ values depending primarily on the temperature and pH of the fluids. As a result, the $\delta^{13}\text{C}$ values measured for CO₂ will change as a higher proportion of the DIC in the pore waters is converted to CO₂. The way in which the $\delta^{13}\text{C}$ values of the CO₂ vary with time and temperature around the heater drift can then be used to place limits on pH and gas transport in the system.

Data

The $\delta^{13}\text{C}$ values of the potential sources of CO₂ in the tunnel were measured. This data is presented in Table 4.7-1. It is significant that the concentrations and $\delta^{13}\text{C}$ value CO₂ from the AO Drift and the Heater Drift are similar. This indicates that the Heater Drift is essentially in equilibrium with the air in the tunnel and that the bulkhead separating the Heater Drift from the tunnel is not limiting gas exchange. It should also be noted that the $\delta^{13}\text{C}$ value of CO₂ measured for rock air is close to the $\delta^{13}\text{C}$ value of CO₂ that would be produced from dissolution of calcite with the $\delta^{13}\text{C}$ value measured for the calcite from the AO Drift. This suggests that the $\delta^{13}\text{C}$ value of CO₂ in the vicinity of the heater drift may have been fairly constant over time.

The $\delta^{13}\text{C}$ values of CO₂ in gas samples collected from the hydrology holes vary depending on both the concentration and temperature of the rock. Figure 4.7-1 is a cross section of the Heater Drift that contains hydrology holes 74-78. The $\delta^{13}\text{C}$ values of CO₂ from gas samples collected during August of 1998 are plotted on this figure along with the temperatures and CO₂ concentrations. The $\delta^{13}\text{C}$ values are highest in samples from nearest the Heater Drift and drop off significantly in samples from further away. Similar patterns were seen in gas samples from the other intervals that were sampled. The variations in the $\delta^{13}\text{C}$ values do not directly correlate with either the temperature measured for the interval sampled or the concentration of CO₂. This is believed to be primarily caused by the large sampling intervals that cross areas with large temperature ranges.

The $\delta^{13}\text{C}$ values of the CO₂ also varied with time. Figure 4.7-2 contains data collected from two of the intervals in the hydrology holes that were sampled over the last 8 months. Interval 77-3 is from the hottest part of the system. By February, the temperature was already greater than 80°C. The CO₂ concentrations were also high and increased to greater than 33,000 ppm (3.3%) by August. By October, the temperatures in this interval had increased past the boiling point of water and the CO₂ concentration had dropped down to 2160 ppm, presumably because the pore waters in the area had boiled away (although,

given the large size of this interval, it is unlikely that the whole region had dried out). The carbon isotope data is consistent with this interpretation. In February, the $\delta^{13}\text{C}$ value of the CO_2 was already much higher than the background, indicating a significant input of CO_2 from pore water DIC. As the CO_2 concentrations increased, so did the $\delta^{13}\text{C}$ values of the CO_2 . When the region began to dry out, the $\delta^{13}\text{C}$ value of the CO_2 decreased slightly (representing CO_2 coming from cooler areas of the system?).

Conversely, interval 57-3 is from a hole that extends above the Heater Drift at ~10 m from the bulkhead. By early October, when the last sample was taken, the temperature of the interval was only 25.5°C. However, the CO_2 concentrations had increased to approximately twice the initial concentration and the $\delta^{13}\text{C}$ values of the CO_2 had dropped down to -16‰. This indicates that CO_2 evolved from pore waters in the hotter areas of the system closer to the Heater Drift is expanding out into the rock, causing CO_2 concentrations in the cooler areas of the system to increase despite no significant increase in temperature. The $\delta^{13}\text{C}$ values of the CO_2 in the cooler areas are decreasing because a significant amount of the CO_2 is being absorbed into the pore waters as DIC. The CO_2 dissolving into the pore waters will have higher $\delta^{13}\text{C}$ values causing the remaining CO_2 to shift to lower $\delta^{13}\text{C}$ values.

Implications

The carbon isotopic data for the CO_2 suggest a couple of initial conclusions. First, the increased concentrations of CO_2 in the rock around the Heater Drift are probably derived from DIC in the pore waters. It is also possible that some of the CO_2 could be from dissolution of calcite in the rock. The second finding is that gas transport around the Heater Drift is relatively fast. In order for the $\delta^{13}\text{C}$ values of the CO_2 to increase as much as they have (from -13‰ to greater than -3‰), the system must be open. In a closed system, the $\delta^{13}\text{C}$ values of the CO_2 could not increase above the initial $\delta^{13}\text{C}$ value of the DIC in the pore waters (approximately -6‰). To rise to greater than -6‰ requires that the initial, lower $\delta^{13}\text{C}$ CO_2 that is evolved from pore water DIC be flushed out of the system. Simple calculations suggest that the residence time of CO_2 in the rock is relatively short (complete turn-over every few days). The only reason such high concentrations of CO_2 are maintained in the rock is because of the much higher starting concentration of inorganic carbon in the pore waters.

Reference

Wigley, T.M.L.; Plummer, L.N.; and Pearson, F.J. 1978. "Mass transfer and carbon isotope evolution in natural water systems." *Geochim. et Cosmochim. Acta* 42, 1117-1139.

Table 4.7-1. Average concentrations and $\delta^{13}\text{C}$ values of CO_2 from the area of the heater drift.

	# of Measurements	ppm CO_2	$\delta^{13}\text{C}_{\text{VPDB}}$ (‰)
1. AO Drift Air	4	430	-10
2. Heater Drift Air	2	420	-10
3. Rock Air ¹	1	900	-13
4. Calcite ²	2		-6

¹ Sample of gas collected from borehole 182 in the

² Data for calcite samples taken from fractures in the AO Drift. The $\delta^{13}\text{C}$ value given is the measured value for calcite. This is different than the $\delta^{13}\text{C}$ value of CO_2 that would be produced from dissolution of the calcite depending on the temperature and the pH of the fluids. At 20°C and a pH of 7, the equilibrium $\delta^{13}\text{C}$ value for CO_2 will be approximately -14‰ (Wigley et al., 1978).

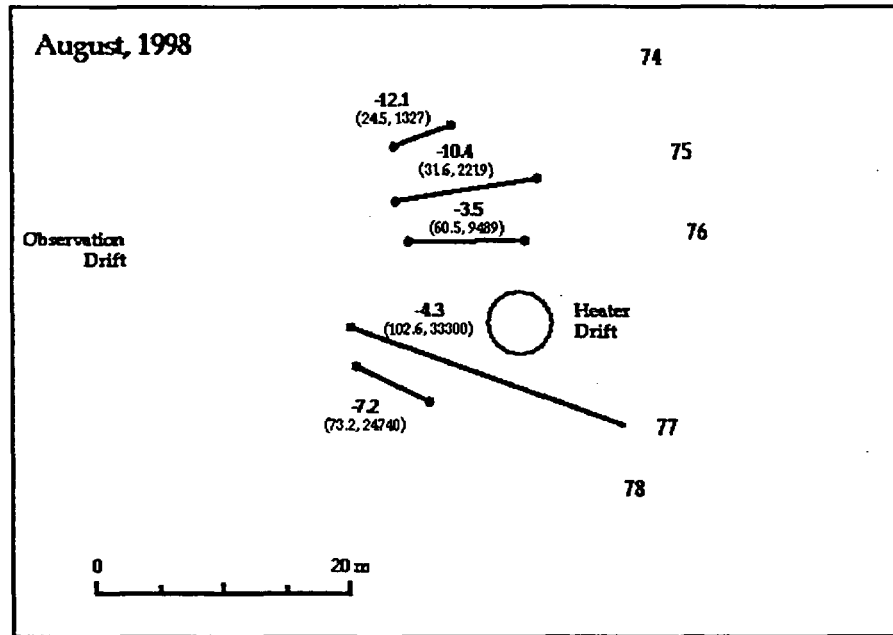


Figure 4.7-1. $\delta^{13}\text{C}$ data for CO_2 (in ‰ units relative to VPDB) in gas samples collected during August of 1998 from Hydrology boreholes around the Heater Drift. Also shown are the temperatures ($^{\circ}\text{C}$) and concentrations of CO_2 (ppmv).

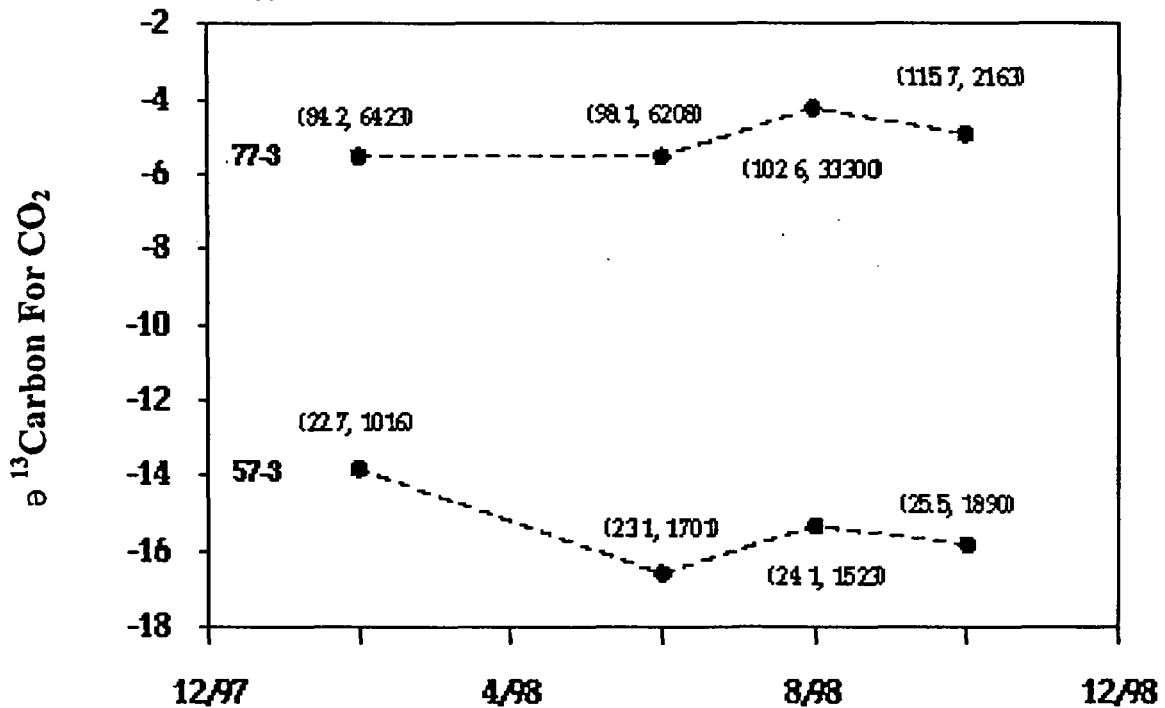


Figure 4.7-2. Plot of $\delta^{13}\text{C}$ data for CO_2 (in ‰ units relative to VPDB) in gas samples collected from intervals 77-3 and 57-3 in the LBNL Hydrology boreholes. Also shown are the temperatures ($^{\circ}\text{C}$) and concentrations of CO_2 (ppmv).

4.8 ANALYSIS OF WATER SAMPLES

The major cation and anion chemistry of the waters recently sampled from the Drift Scale Test has been analyzed. Several water samples were obtained from the hydrology holes, and pads contacting wet borehole walls were collected from the liners installed in the chemistry boreholes. An aqueous sample was also collected from one of the chemistry boreholes during gas sampling.

The samples were all analyzed with respect to the cations Si, Na, Ca, Mg, Sr, Al, K, Fe, S, B, and Li by the method of Inductively-Coupled Plasma and Atomic Emission Spectrometry (ICP/AES). The anion analyses performed by Ion Chromatography (IC) included F, Cl, Br, NO₂, NO₃, PO₄, and SO₄. A field measurement was also made of pH and temperature in most instances at the time of collection.

Water Samples Collected From The Drift Scale Test

Aqueous samples have been collected from the hydrology boreholes where packed-off intervals separate zones open to the borehole walls. To date, water has been sampled from two of these hydrology boreholes: borehole 60 and borehole 77 occupy corresponding positions in two different borehole arrays. Both boreholes are collared in the observation drift, run normal to the heater drift plane, and angle downward and below the heaters. The first water from the hydrology boreholes was taken 6 months after heater turn-on, in two zones of borehole 60. Samples were collected again from these zones and from borehole 77 about 2 months later.

Water samples taken for chemical analysis from the chemistry boreholes were first collected in April of 1998 (~4 months after the start of heating). At that time the first absorber liner was removed from borehole 55, and the attached absorber pads were collected for analyses. This borehole corresponds in orientation and position within its borehole array to the two hydrology holes from which the previously described water samples were taken. The absorbent pads installed on the liner were positioned every 4m along the length and all appeared to be saturated. One pad, however, located ~18m into the hole was beginning to show signs of drying. Another liner was pulled in June, and again all the pads appeared to be wet. The second liner was pulled from borehole 56, the borehole immediately below 55. In the case of liner 56, the pads visually did not appear to be as wet as for those collected from 55.

Liquid water was also collected on one occasion from the chemistry boreholes. During gas sampling, an in-line water trap collected ~30 mls of water as air was pumped from the gas sampling ports to the analysis unit. This water came from borehole 54, within the same array of chemistry holes as 55 and 56, but which is angled upward and immediately above the heaters in the drift. The sampling port which yielded water was located almost at the end of the borehole, at a distance of ~35m in from the collar. This water was collected for sampling and analysis, but it was unexpected, and a formal sampling protocol had not been established.

Sample Handling and Processing

The borehole water samples from the hydrology holes were collected and filtered through a 0.45 µm pore filter. These water samples were stored in polyethylene containers and were either immediately stabilized with HNO₃ for sample splits designated for cations, or the containers simply went into refrigerated storage until they could be sent for analyses. The controlled thermal conditions were unable to be maintained throughout the entire shipping and transfer process, however.

The sample collection of absorber pads included the immediate removal from the retrieved borehole liner and storage in clean, air-tight polyethylene bags. A visual examination showed that the pads suffered from gross contamination of rock and soil particulates that could not easily be excluded during processing in the lab and therefore introduced significant uncertainty into the analytical results. Another potential contaminant was the pervasive presence of mildew on the pads.

Analytical Chemistry Results

The measured cation and anion chemistry of the aqueous samples are reported in Table 4.8-1. Hydrology hole samples are identified by the borehole number and the zone. The chemistry hole sample is identified by the borehole number and the gas sampling port number. In addition to this identification descriptor, all samples have also been given a YMP bar code for sample tracking which is reported as the SMF number. The table includes the sample collection date and field measured values of pH, temperature, and Br concentration if available. All the samples have a Q-pedigree, except for the chemistry borehole water, 54-1. All the analytical data are qualified.

The pad data that have been collected to date are not reported. As previously mentioned, the pads were recognized to be contaminated, and although efforts were made to reduce the contamination from areas analyzed, results are suspect. Additional analyses were also performed to understand the contribution to background levels that the pad generates. These analyses revealed significant heterogeneity of several of the analytes, further complicating the interpretation of potential geochemical changes with respect to depth or distance from heaters. Further examination of the results will determine if some of the data can be utilized.

Discussion

Several liters of water were collected from the hydrology hole #60. The water chemistry in both zones 2 and 3 is inconsistent with a simple condensate which has no history of rock/water interaction. On the other hand, the chemistry of water collected from borehole 77-3 was different; it was dilute by comparison. The temperature readings recorded for 77-3 was 102.8 °C which was generally hotter than the other zones from which water was collected. This borehole yielded only about 200 mls of water, and one possibility is that the sample is simply water vapor stripped from the gas as the hot air is pumped into the cooler atmosphere of the observation drift. At any rate, it is not comparable to the chemistry of the other waters sampled. Finally, borehole 54 port 1 yielded water which also does not appear to be simple condensate. Because its chemistry is suspect, however, since the process of filtration and flushing of the lines were not employed, the results should not be used to make geochemical interpretations. Instead, it may be useful to understand moisture distribution within the test, and to plan for the possibility of future water collections via the same process.

Table 4.8-1. Thermal test water chemistry.

SMF number	Suite 1 ^{mol}	Suite 1 ^{mol}	Suite 2 ^{mol}	Suite 2	Suite 2	H2O trap
	SPC00527969	SPC00527977	SPC00527915	SPC00527916	SPC00527917	SPC00530268
collection date	06/04/1998	06/04/1998	08/12/1998	08/12/1998	08/12/1998	06/04/1998
temp (C)	36.2	82.1	60.2*	91.6*	102.8*	
field pH	7.5	7.7	6.9	6.8	5.5	7.32
field Br (ppm)*	0.75	0.96	0.385	0.345	0.392	
Na (mg/l)	20.0	24.0	20.4	17	2.4	27.0
Si (mg/l)	56	41	51.8	44	1.48	509
Ca (mg/l)	20	25	19.9	19	2.09	28.8
K (mg/l)	6.0	4.5	5.4	4.5	1.4	n.d. < 0.5
Mg (mg/l)	2.9	5.7	1.21	4.0	0.21	5.79
Al (mg/l)	0.12	n.d. < 0.06	n.d. < 0.06	n.d. < 0.06	n.d. < 0.06	n.d. < 0.06
B (mg/l)	1.2	0.92	1.84	1.1	0.13	1.71
S (mg/l)	5.5	9.2	4.5	5.2	1.4	16.6
Fe (mg/l)	0.04	n.d. < 0.02	0.02	0.12	n.d. < 0.02	n.d. < 0.02
Li (mg/l)	0.07	0.07	0.03	0.04	n.d. < 0.01	0.07
Sr (mg/l)	0.18	0.34	0.11	2.2	0.05	0.4
F (mg/l)	1.00	0.82	0.71	0.43	nd < .007	1.00
Cl (mg/l)	10 1.0×10^{-4}	16 4.5×10^{-4}	6.14 1.7×10^{-4}	5.52 1.6×10^{-4}	2.15 6.1×10^{-5}	31.0
Br (mg/l)	0.84	0.73	0.05	0.21	nd < 0.03	n.d. < 0.02
SO4 (mg/l)	17 1.8×10^{-4}	30 3×10^{-4}	4.88 5.1×10^{-5}	8.81 9.2×10^{-5}	1.86 1.9×10^{-5}	45.0
PO4 (mg/l)	n.d. < 0.07	n.d. < 0.07	0.25	0.16	1.06	n.d. < 0.07
NO2 (mg/l)	n.d. < 0.01	n.d. < 0.01	nd < 0.04	nd < 0.04	nd < 0.04	n.d. < 0.01
NO3 (mg/l)	3.00 4.8×10^{-5}	3.6 3.8×10^{-5}	0.46 7×10^{-6}	0.6 9.7×10^{-6}	0.22 3.5×10^{-6}	9.00

* These temperatures were downloaded from the data collection system, and are not a measured fluid temperature at the time of collection.

The water sample from borehole 54-1 is not "q" and the analyses likely reflect contaminated sample

	60-2	60-3	60-2	60-3	77-3	54-1
$\frac{[NO_3] + [SO_4]}{[Cl]}$	0.81	0.75	0.34	0.64	0.37	

4.9 Acoustic Emission / Microseismic

Sixteen accelerometers are installed at various locations in the Drift Scale Test block to monitor micro-seismic or acoustic emissions (AE). Micro-cracking due to heating is thought to be caused by acoustic emissions. Shear movement and rock fracturing are also expected to release micro-seismic emissions. Travel time data to multiple accelerometers can be processed to locate a particular event in space. This information may then be correlated with some of the other measurements such as rock displacement. This information may be useful in understanding the process(es) taking place in the rock.

Three of the sixteen accelerometers are malfunctioning. The remaining thirteen are still adequate for isolating and locating an event. The system is subject to severe interference due to noise from any of the many other electrical systems in the DST.

After the heating started, the AE system in the DST was experiencing both severe noise interference and actual events making it difficult to isolate and locate any event in time and space. One event, considered to have been isolated, took place on January 7, 1998. The processing of the data to locate it is expected to be completed in the near future.

Recent installation of a filter to eliminate high frequency noise and a trigger selection box which will not trigger the system if emissions reaches multiple accelerometers exactly at the same time is expected to greatly help in isolating events.

4.10 Video Imaging Inside the Heated Drift

The Camera System in the Drift Scale Test is intended to periodically take both video and infrared images inside the Heated Drift. Baseline images were collected before the start of heating in December 1997. The infrared (IR) images after the start of heating did not allow any distinctive features to be identified. This is thought to be due to extremely low temperature gradient on the surfaces being imaged. IR imaging may be useful during the cooling phase to identify any moisture vapor escaping into the Heated Drift from fractures, if there is any such event and the temperature difference between the moisture and rock surfaces in the vicinity is finite and distinguishable by IR imaging.

Video images of the inside of the Heated Drift have been collected in March, July and November of 1998. No changes of any significance has so far been noted.

4.11 Moisture Movement Across the Bulkhead

The Heated Drift is separated from the rest of the thermal testing facility by a bulkhead. The bulkhead is a thermal bulkhead, not a pressure bulkhead. It is made of a steel frame and steel plates and carries the lighting fixtures, viewing windows and the camera door. The bulkhead is insulated on both sides by fiber glass insulation pads.

The relative humidity (RH) inside the Heated Drift dropped to approximately 15 percent during the first 10 days of heating. Thereafter, the RH inside the HD fluctuated between 10 and 25 percent with a peak to peak interval of approximately 4 days. Measured RH in the HD has been inversely tracking the air pressure in the drift. After some forty days of heating, moisture started to flow out of the Heated Drift as evidenced by condensation on various surfaces near the bulkhead and the formation of a puddle on the floor. Such wet conditions near the bulkhead alternated with dry conditions with the latter coinciding with low RH inside the HD.

The Drift Scale Test System, comprised of the HD and the surrounding heated and unheated rock, is not a closed system. The DST block is exchanging moisture and air with its surroundings through the bulkhead and the fractured rock. Outflows coincide with higher RH in the HD and lower barometric pressure.

As the rock immediately surrounding the drift is heated to above the boiling temperature, the pore water in the rock is mobilized and driven outward creating a dry-out zone around the drift. As the mobilized water in the vapor phase moves outward, it condenses when it reaches cooler regions and vaporizes again, as additional thermal pulse reaches it. A boiling zone is thus formed around the dry-out zone. Phase changes occur continuously in the boiling zone causing pressure to build up. When the barometric pressure and the pressure inside the HD are high, steam and water is confined to the boiling zone. When the barometric pressure and the pressure in the HD drop, steam and water escape from the boiling zone moving into the HD via the fractures and causing the RH in the drift to rise, much like what happens in pressure cooker or geyser.

Ways of measuring the heat loss through the bulkhead, both by conduction and convection, have been investigated. A pair of sensitive heat flux meters has been acquired and will be used to measure the heat loss by conduction in the first part of January 1999.

Measuring the loss by convection is difficult and complicated because flow takes place at numerous locations, at various rates and at different temperatures. A system employing mass flowmeters and mass spectrometers *is being investigated.*

4.12 THERMAL-HYDROLOGIC ANALYSIS

An interpretive analysis of the thermo-hydrological processes of the Drift Scale Test (DST) at Yucca Mountain was conducted by studying measured temperature data collected in the first 9 months of heating and comparing them with simulated results from the 3-D DST numerical model. In this model, fractures and matrix are each represented as a continuum for flow of liquid, gas and heat. The effective continuum approach (ECM) is applied in three-dimensional simulation runs, while the dual permeability formulation is used for certain two-dimensional runs to study model sensitivity to the fracture-matrix interaction concept. The numerical simulation is exercised for two different infiltration rates—the best estimate of 3.6 mm/yr for the location of the heater, and one-tenth of the expected estimate, 0.36 mm/yr—in order to include a full range of plausible responses. Infiltration is assumed to be constant in time; no episodic events are considered. Model properties are estimated from site-specific measurements whenever possible, otherwise adopted from UZ site-scale model results. Two alternative data sets are used for the DST, one associated with 3.6 mm/yr percolation, the other associated with 0.36 mm/yr percolation. The computational grid designed for the DST honors the designed test conditions as closely as possible, using a total number of 48,249 gridblocks and 157,474 connections between them (Figure 4.12-1).

The model used for the DST simulations is based on the three-dimensional predictive model developed by LBNL in 1997 (Birkholzer and Tsang, 1997). The predictive simulations were carefully reevaluated based on the first 9 months of data, and, as a result, several model refinements have been made. In general, such model refinements can be categorized as follows:

- 3 Modification of test conditions and geometry
- 3 Modification of model conceptualization
- 3 Modification of model rock properties

So far, we have focused on the first two items, i.e., a better representation of the actual test conditions, and a review of the conceptual model. The following model improvements were made:

- 3 Heater power and schedule were adjusted to 77% of maximum power for the canister heaters and 94% of maximum power for the wing heaters, representing the average measured heater power in the DST for the first 4 months of heating
- 3 The concrete invert in the Heated Drift, originally not represented by the model, was added to the computational grid.
- 3 The bulkhead boundary condition was modified to allow for gas transport between the hot and the cold side of the heated drift.
- 3 The initial temperature and moisture conditions close to the Heated Drift were adjusted to account for the impact of elevated drift temperature and drift ventilation prior to heating.

Our observation so far is that the simulation results for the first 9 months of heating compare favorably with temperature data as well as with results from active hydrological testing. The model refinements all contribute to a better match between simulation results and field data, in particular the introduction of the gas-permeable bulkhead boundary condition. Our results also indicate that thermal radiation is quite effective within the Heated Drift, and can be approximated in the model by assuming totally effective black body heat radiation. Simulation runs performed for a heating period of several years show that the current heater power can probably be maintained for about 24 months of heating before the wall temperature in the Heated Drift reaches 200°C (Figure 4.12-2).

So far, no model calibration has been performed. Sensitivity studies, however, indicate that the temperature match between measured and simulated results may be further improved by using adjusted rock property sets. Hence in future modeling efforts, the model properties for the DST will have to be carefully evaluated. Sensitivity studies have also been conducted to study the impact of model conceptualization, i.e., the validity of ECM or DKM approaches, respectively. The simulated temperatures are almost identical for the two model concepts; however, obvious differences between ECM and DKM are obtained for saturation results, as the DKM method promotes gravity-driven liquid flux in the fractures (Figure 4.12-3). We may conclude from this analysis that temperature data will probably not diagnostically discriminate the ECM and DKM concepts in the DST. However, we believe that a thorough analysis of the air-permeability tests

performed in different borehole intervals at different heating phases could provide such information, since the ECM and the DKM modeling concept clearly results in different fracture saturation fields. Further analysis of the different modeling concepts will be performed in future studies.

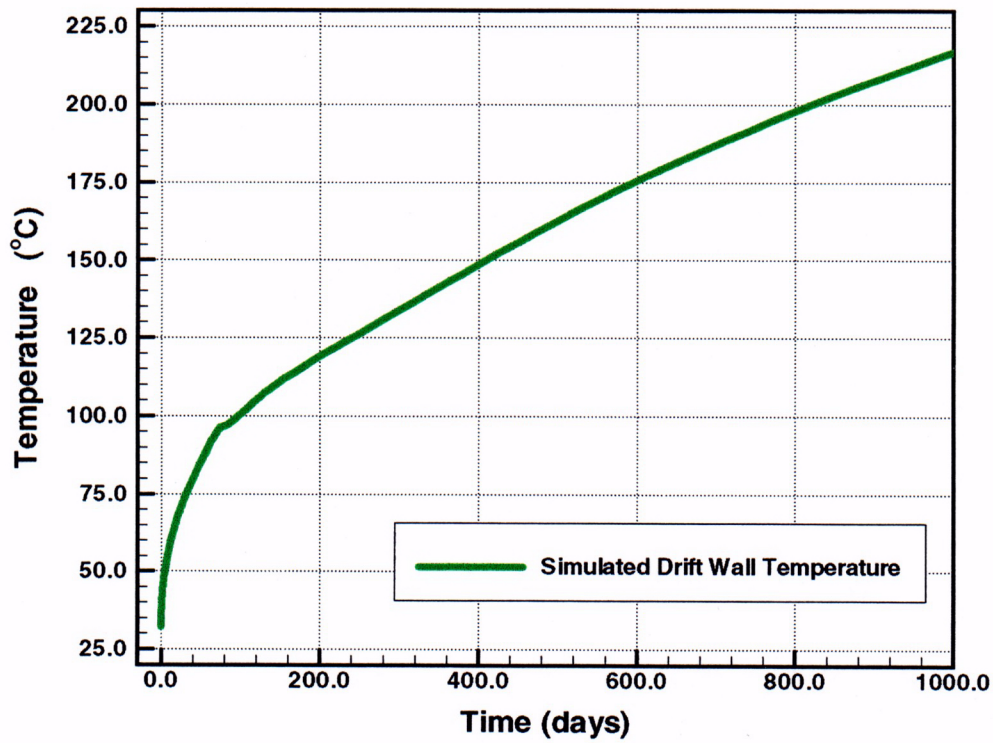
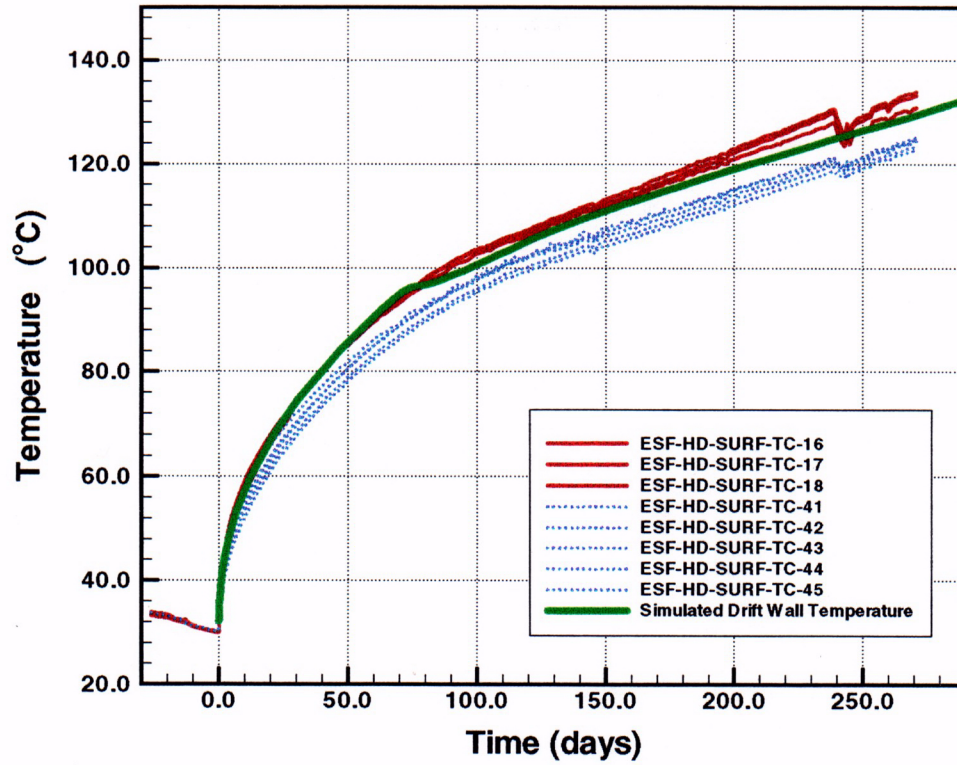


Figure 4.12-2. Measured and simulated temperature evolution at the Heated Drift wall. Measured temperature is shown at two different cross sections along the Heated Drift.

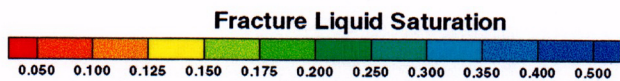
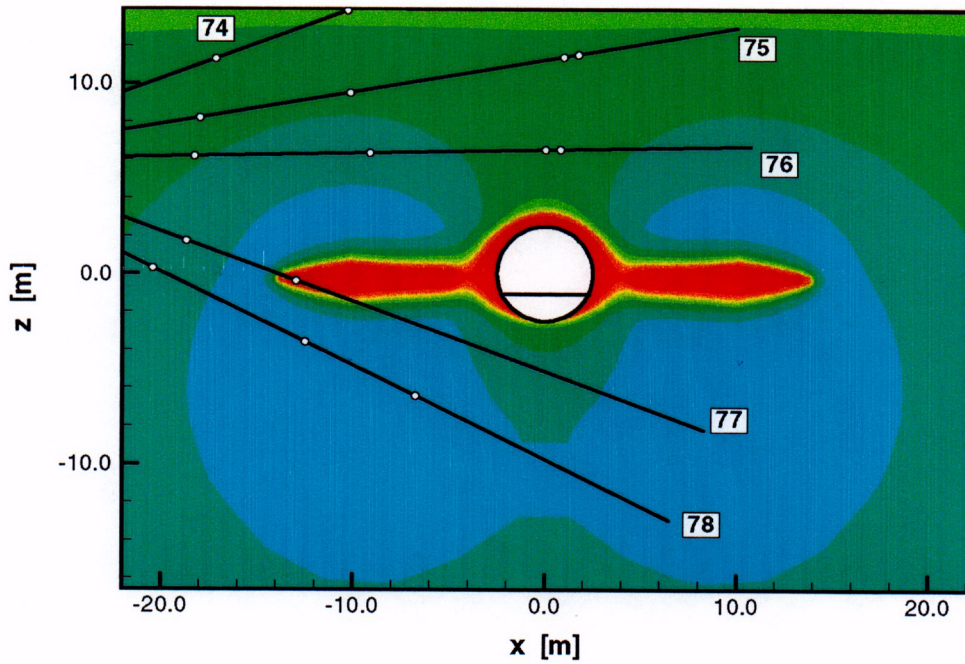
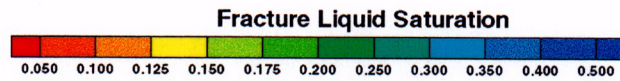
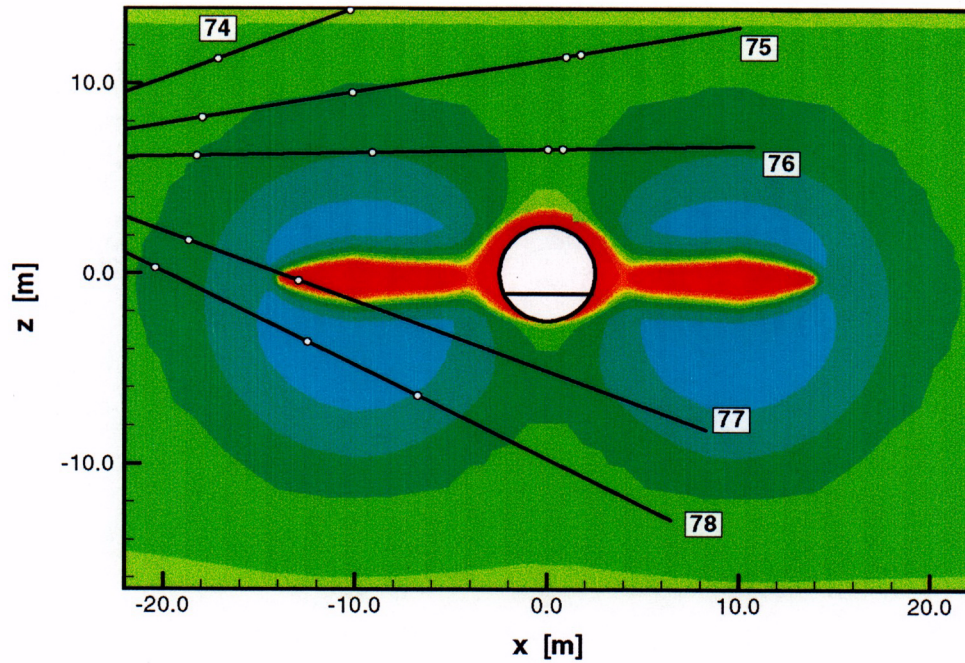


Figure 4.12-3. Fracture liquid saturation at 3 months of heating, using an ECM representation (top) and a DKM representation (bottom). Saturation contours are presented in a vertical cross section with hydrology boreholes 74 through 78,

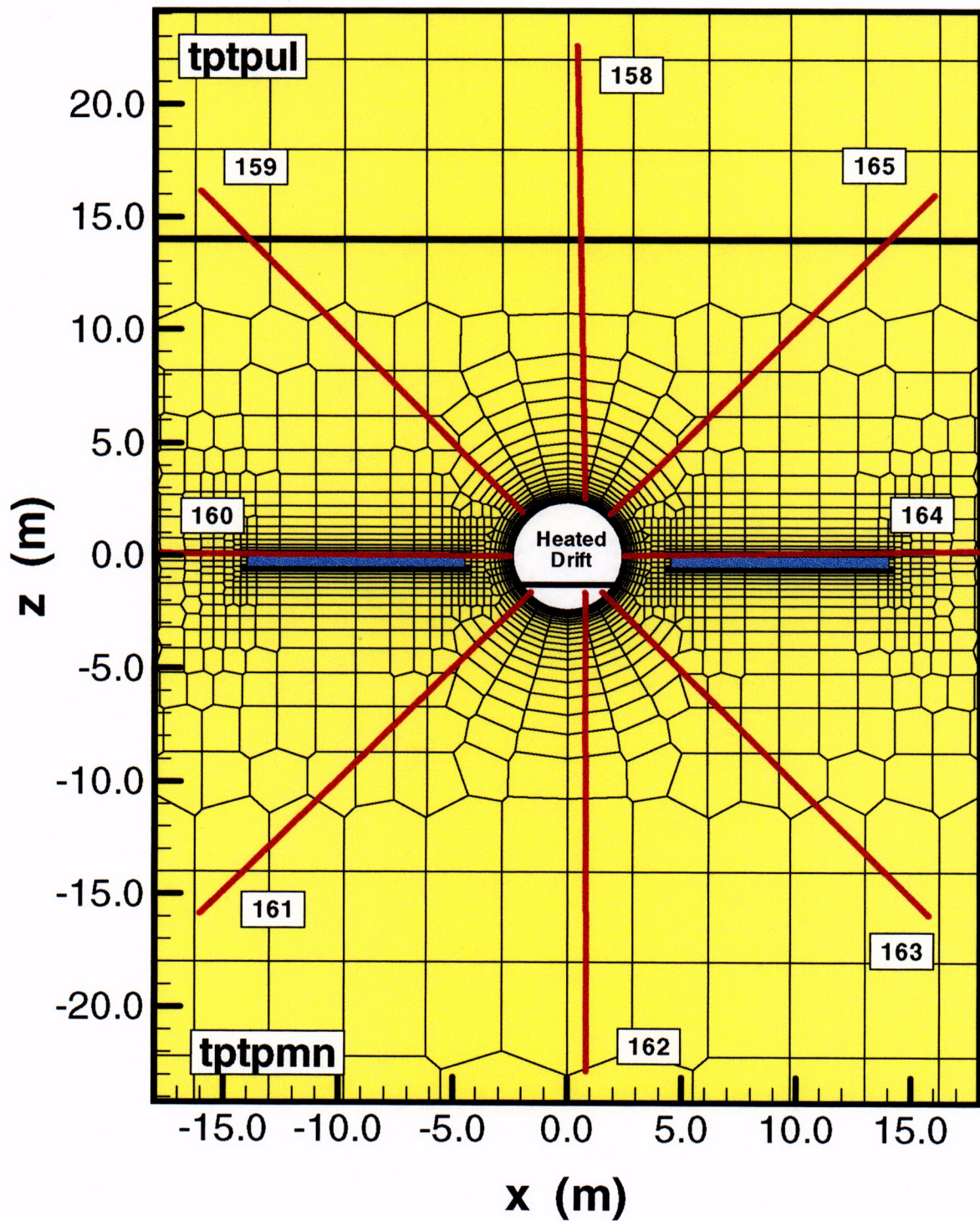


Figure 4.12-1. Close-up view of model grid in a vertical cross section at $y = 23$ m from the bulkhead with RTD borehole 158 through 164. The blue area indicates location of wing heaters.

C-21

4.13 THERMAL-CHEMICAL ANALYSIS

The modeling of THC processes for the DST included updates to the chemical model and sensitivity studies on the effects of increased fracture porosity. New gas measurements allowed for some qualitative comparisons to the model results. Refinements of the model included the consideration of CO₂ degassing and transport for full heating and cooling phases of the DST.

Model results show a large region of increased partial pressure of CO₂ (PCO₂) beyond the heat pipe zone into areas of near-ambient temperatures. Because of the dissolution of the CO₂ into the aqueous phase the pH of fracture waters in these areas has declined from 8.2 to a minimum of about 6.9. Except for one anomalous water sample, having a pH of 5.5, this agrees favorably with the waters that have been collected from boreholes. The increased PCO₂ also agrees qualitatively with measurements from gas samples taken from the hydrology holes. Direct comparisons between model results and measured data is limited by the large packer intervals from which the gas samples are taken, where large spatial gradients in chemistry and temperature are predicted.

The model results indicate that dissolution of cristobalite on fracture walls occurs predominant in the high temperature region of the condensate zone (approximately 90 to 95 degrees C). Most amorphous silica precipitation takes place in an even narrower region at the boiling front and closer to the heater than the center of the cristobalite dissolution region. Calcite dissolution in fractures takes place over a wider area as it is related to the decreased pH due to increased PCO₂, and the drainage of lower pH waters into cooler fractures below the heated area. Calcite precipitation is dominant near the drift wall and along the wing heaters owing to its reverse solubility with increasing temperature. The drainage of more dilute condensate waters below the drift is also shown clearly by the chloride concentrations in fracture waters below the drift

Modifications of the "base case" fracture porosity by factors of 5 and 10 were done to evaluate the uncertainty in the THC calculations due to the possibly higher fracture porosities indicated by in-situ tracer testing. While not changing the overall behavior of the system, an increased fracture porosity leads to lower liquid saturations in fractures below the drift and modified water chemistry in the high temperature condensate region. In the most dilute region, chloride concentrations are a little higher for the larger fracture porosity case whereas silica concentrations are significantly higher.

4-14 Heating Plan

The heating phase of the DST was initiated in December 1997 with the wing heaters at 100% of full capacity i.e a total of approximately 143 kW and the canister heaters at 80% of design capacity i.e 6 kW per canister for a total of 54 kW. There were three principal objectives behind the heating plan. These were : a) drift wall temperature not to exceed 200°C; b) a volume of over 10,000 cubic meters of rock to be heated above 100°C; and c) a boiling zone at approximately 95°C will be maintained for approximately 3 years.

Modeling analysis before the start of heating had indicated that with the above power outputs from the heaters, drift wall temperature will reach 200°C in approximately 12 to 14 months. Actual heater power during the first year of heating has averaged approximately 188 kW and some heat loss has been taking place through the bulkhead. The rate of rise of the drift wall temperature has slowed down in recent months with the drift wall temperature at the end of November 1998 at approximately 154°C. The models have been refined based on measured temperatures. Recent modeling indicates that it will take some 20 to 22 months of heating at the current heater power setting for the drift wall temperatures to reach 200°C.

The idea that the heater outputs may be adjusted so that the temperature goals are met sooner, was thoroughly discussed in the October 1998 workshop in Livermore. The consensus was that no adjustment to the heater outputs will be made even though 200°C drift wall temperature may not be attained for another year or so. It was decided that the matter will be reconsidered in 10 to 12 months and adjustments to heater powers will be made if deemed necessary at that time.

The goal of 200°C drift wall temperature was adopted before the start of the heating phase with the expectation that increase in the coefficient of thermal expansion due to phase changes of silica polymorphs may manifest and be observed. However, it is now known that phase changes from cristobalite and trydamite do not occur below 230°C. Thus, the goal of 200°C drift wall temperature was considered unnecessary. Consultation with the repository designers on the other hand indicated that they would like to maintain the goal of 200°C drift wall temperature to observe the stability and integrity of the drift at these elevated temperatures. Maximum drift wall temperature of 200°C, therefore, remains a goal of the DST.

4.15 UPDATING THERMAL TEST STRATEGY

This presentation dealt with the issue of revisiting and ultimately updating the strategy for the DST. Basically, the presentation was divided into three categories: background discussion, the need for a strategy update, and a proposed framework. Background discussion related to the current thermal test strategy as delineated in the report entitled "Updated In Situ Thermal Testing Program Strategy" released in April, 1997. Much of the strategy in that document related to evaluation of specific thermal tests ranging from laboratory testing to a large-scale, long-duration thermal test. Specific details and methodologies such as those corresponding to the 8-year duration of the DST were beyond the scope of this report. Experiences gained from the near completion of the SHT and LBT were also part of the background discussion.

The need for an update to the DST strategy was the second category in this discussion. Factors cited included pre-occupation with the planning, implementation, and early stages of the DST, the comparatively long duration of the test, shortcomings of adhering to the strategy applied to the SHT and LBT, merit of developing a consensus among the TTT, the possibility of the DST becoming a major component of DECOVALEX III, and the benefit of producing a written document with details of the process and its linkage to key program milestones.

The last category dealt with a proposed framework from which to develop an updated strategy to the DST. Components presented included the consideration of various levels of couplings (e.g. one-way, two-way, and full), a process that integrates TTT resources, the interaction with the group responsible for development of near-field process models, and the notion that updating the DST strategy will be an iterative process. Discussion concluded with an agreement to schedule a full-day meeting with PIs, POCs, and technical leads to begin the process of producing a more comprehensive strategy for the DST.

4.16 DRIFT SCALE TEST and DECOVALEX

DECOVALEX is an international consortium of governmental agencies associated with the management/disposal of high level nuclear waste and spent nuclear fuel in Canada, Japan, Finland, France, Spain, Sweden, and the United Kingdom. DECOVALEX stands for DEvelopment of COupled models and their VALIDation against EXperiments, signifying the overall objective of the consortium. The United States Nuclear Regulatory Commission participated in the first DECOVALEX project, DECOVALEX I, which was from 1992 to 1995. DECOVALEX II, underway since then, is scheduled to be completed in March 1999. Meanwhile, DECOVALEX III is being organized at this time and last summer the Department of Energy applied to join the consortium with the proposal that the Drift Scale Test be a test case for DECOVALEX III.

In November 1998, the consortium invited DOE to join DECOVALEX. The DOE has since decided to participate in DECOVALEX III. The consortium is planning to perform four tasks in DECOVALEX III. These are:

Task 1. Numerical simulation of the FEBEX in-situ THM experiment in Switzerland, proposed by ENRESA, Spain.

Task 2. Numerical simulation of the Drift Scale Test, proposed by the Yucca Mountain Site Characterization Office, DOE, USA.

Task 3. Treatment of coupled THM processes in performance assessment (PA) of Repositories, based on a number of suggestions from DECOVALEX II participants.

Task 4. A forum for outside PA experts to be invited to interact with DECOVALEX III participants to discuss application of THM process models in the performance assessment in other projects.

Organizational meetings for DECOVALEX III are scheduled in January and March, 1999. Actual work is not expected to start until the second half of FY 1999.

DRAFT DISCLAIMER

This contractor document was prepared for the U.S. Department of Energy (DOE), but has not undergone programmatic, policy, or publication review, and is provided for information only. The document provides preliminary information that may change based on new information or analysis, and is not intended for publication or wide distribution; it is a lower level contractor document that may or may not directly contribute to a published DOE report. Although this document has undergone technical reviews at the contractor organization, it has not undergone a DOE policy review. Therefore, the views and opinions of authors expressed do not necessarily state or reflect those of the DOE. However, in the interest of the rapid transfer of information, we are providing this document for your information.

Sardi,

*This should go to Brit Leslie,
& others tracking Drift Thermal
Test.*

Chad

TRW Environmental
Safety Systems Inc.

1261 Town Center Drive
Las Vegas, NV 89134
702.295.5400

*Patterson
Deb*

TRW

QA: N

Contract #: DE-AC01-91RW00134
LV.NEPO.LRH.01/99-034
January 4, 1999

Dennis R. Williams
Deputy Assistant Manager for Licensing
U.S. Department of Energy
Yucca Mountain Site Characterization Office
P.O. Box 30307
North Las Vegas, NV 89036-0307

Dear Mr. Williams:

Subject: Thermal Test Progress Report No. 1

I am pleased to transmit herewith the Thermal Test Progress Report No. 1 which is the first of a series of informal reports to be prepared every three months. This report has been prepared following the Sixth Thermal Test Workshop held at Livermore in October 1998. These progress reports are intended to help communicate the progress of the in-situ thermal tests, are not a Level 4 or 3 baseline commitment and should be considered draft in nature. Therefore, they are not subject to the provisions of the CRWMS M&O YAP 30.63 (Submittal, Review, and Acceptance of Deliverables) and should not be used in support of/or cited in QA activities.

Should you have any questions, please feel free to contact Robin Datta of my staff at (702) 295-5741 or me at (702) 295-5604.

Sincerely,

Larry R. Hayes

Larry R. Hayes, Manager
Natural Environment Program Operations
Management and Operating Contractor

cc:
R. E. Spence, DOE/YMSCO, Las Vegas, NV
R. L. Patterson, DOE/YMSCO, Las Vegas, NV
Deborah Barr, USGS, Las Vegas, NV
M. T. Peters, M&O, Las Vegas, NV

MAIL - 2

RECEIVED
JAN - 5 1999